Endogenous noise of neocortical neurons drives atypical sensory response variability in autism

Arjun Bhaskaran
Mac Gill University https://orcid.org/0000-0002-0332-2430
Théo Gauvrit
INSERM U1215 https://orcid.org/0000-0003-4563-6929
Yukti Vyas
INSERM U1215
Guillaume Bony
INSERM U1215
Melanie Ginger
Neurocentre Magendie
Andreas Frick (andreas.frick@inserm.fr)
INSERM, Neurocentre Magendie https://orcid.org/0000-0002-1392-0995

Article

Keywords: Atypical sensory experience, autism, fragile x syndrome, Fmr1-/y mice, neocortical circuits, neural noise, variability, preclinical models, sensory processing, neurophysiological biomarkers

Posted Date: March 20th, 2023

DOI: https://doi.org/10.21203/rs.3.rs-2572651/v1

Additional Declarations: There is **NO** Competing Interest.

Version of Record: A version of this preprint was published at Nature Communications on November 30th, 2023. See the published version at https://doi.org/10.1038/s41467-023-43777-z.

Abstract

Excessive trial-by-trial and inter-individual neural variability of sensory responses are hallmarks of atypical sensory processing in autistic individuals with cascading effects on other core autism symptoms. The neurobiological substrate of this exaggerated variability is unknown. Here, by recording neocortical single neuron activity in a well-established mouse model of autism, we characterized atypical sensory processing and probed the role of endogenous noise sources as a driver for response variability. The analysis of sensory stimulus evoked activity and spontaneous dynamics, as well as neuronal features, reveals a complex phenotype composed of both cellular and circuit alterations. Neocortical sensory information processing in autistic animals is more variable, unreliable, and temporally imprecise. This increased trial-by-trial and inter-neuronal response variability is strongly related with key endogenous noise features. We provide a novel preclinical framework for understanding the sources of endogenous noise and its contribution to core symptoms in autism, and for testing the functional consequences for mechanism-based manipulation of this noise.

Introduction

Accurate neural processing of sensory information is fundamental for human perception, higher cognitive abilities, and interaction with our environment. Individuals with autism spectrum disorder (ASD) commonly report differences in their perception of sensory information. This altered sensory perception has cascading effects on, and is predictive of, other core autism symptoms [1, 2, 3] Consequently, sensory symptoms are now included as a core diagnostic criterion for ASD in the Diagnostic and Statistical Manual of Mental Disorders [4]. However, there is a paucity of preclinical studies investigating the neurobiological underpinnings of atypical sensory response variability in autism [5].

Excessive inter-individual and trial-by-trial variability of neural responses are hallmarks of noisy sensory processing in autistic individuals [6, 7, 8, 9, 10, 11, 12]. An emerging model suggests that exaggerated variability of sensory evoked responses is the result of a “noisy” brain state, rendering sensory information processing more variable and less reliable, as shown by clinical studies [6, 7, 13, 14, 15, 16]. Consequently, autistic individuals exhibit marked heterogeneity in their perception and responsiveness to sensory input [3, 17] and temporal sensory processing issues [18, 19]. Altered sensory perception also affects situational predictions that are based on prior sensory experience [8].

The concept of “noise”, however, is poorly defined for the field of clinical neuroscience. This makes describing its underlying mechanisms and their relationship with atypical sensory information processing challenging [7, 9, 15, 16, 20, 21, 22, 23]. In addition, tests of the sources and constituents of endogenous neural noise and its consequences for sensory information processing remain incomplete in human experiments due to the limited resolution of non-invasive, large-scale physiological measures [23, 24].

Here, we consider the hypothesis that internally generated or endogenous neural noise drives atypical sensory response variability. We use the term endogenous noise to describe core neural parameters that

emerge from mechanism-derived alterations in cellular or network properties. To overcome the aforementioned limitations and to test our prediction, we turned to the *Fmr1*$^{-/y}$ mouse, an established mouse model for sensory symptoms in ASD [25]. We recorded the activity of individual neurons of the primary somatosensory cortex (S1) processing touch-related sensory information We focused on paw-related tactile sensory information given that this sensory modality is directly translational due to its high comparability between humans and mice [26]. Moreover, touch is one of the most frequently affected sensory modalities in autism [1, 2, 3], and the earliest sense to develop, providing a vital means for children to explore the world and exchange social contact with parents and caregivers [27, 28]. Our approach enabled us to provide a detailed picture of atypical tactile sensory information processing in the neocortex and to identify changes in key properties of cellular and network function. We then explored to what degree these alterations contribute to enhanced endogenous neural noise, and the link between endogenous noise and autism-associated variability in sensory information processing.

Results

To explore whether the complex features of atypical sensory information processing described in clinical studies can be recapitulated in a preclinical model, we measured the processing of tactile sensory information in individual neurons of the primary somatosensory (S1) cortex in anaesthetized *Fmr1*$^{-/y}$ mice. Tactile stimuli were given to the contralateral hind-paw (HP) or forepaw (FP) (Fig. 1A and Fig. 3N). Pyramidal neurons were whole-cell recorded from layer (L) 2/3 (Fig. 1A) — a neuron type that controls the gain of sensory-evoked responses [29] and that is preferentially affected in ASD [30].

Trial-by-trial variability of sensory responses is markedly increased in S1–L2/3 pyramidal neurons of Fmr1$^{-/y}$ mice

First, we explored whether the increased trial-by-trial neural variability observed in human studies [6]) is also a hallmark of sensory responses in *Fmr1*$^{-/y}$ mice. Thus, we compared tactile HP stimuli-evoked excitatory postsynaptic potential (EPSP) responses to 40 repetitions of the same stimulus in S1–HP neurons of *Fmr1*$^{-/y}$ and WT littermate mice (Fig. 1B and C for examples). As expected, WT neocortical neurons responded with a typical level of trial-by-trial variability to repeated stimuli (Fig. 1B–E; [31, 32]). In contrast, this variability was markedly elevated in *Fmr1*$^{-/y}$–L2/3 pyramidal neurons. It was increased for both the amplitude (Fig. 1D; $p < 0.01$), half-width (Fig. 1E; $p < 0.01$), and slope (Table S1) of the EPSPs, thus affecting the magnitude as well as temporal features of sensory information processing from trial to trial. Due to this greater trial-by-trial variability (i.e. noise), the signal-to-noise ratio (SNR, [6]) of the EPSP amplitudes was below that of WT neurons (Fig. 1F, $p < 0.05$). Given that this variability is likely shared across many neurons of the S1–L2/3 network [33], the reliability of neocortical sensory information processing might be severely constrained in these mice.

In addition, the range of EPSP amplitudes evoked by HP stimulation (Fig. 1G), and the mean value (Fig. 1H, $p < 0.001$) were both greater in *Fmr1*$^{-/y}$ neurons, significantly increasing the possible outcome of

tactile stimulus evoked responses in these neurons. The larger mean amplitude was also accompanied by a steeper slope (Fig. 1I, $p < 0.05$) and a faster onset of the responses following HP stimulation in *Fmr1*$^{-/y}$ neurons (Fig. 1J, $p < 0.001$). Moreover, the EPSPs were prolonged (increased EPSP half-width, Fig. 1B and K, $p < 0.001$), indicating a broader temporal window for synaptic integration [34].

Our findings demonstrate that tactile stimuli elicit highly variable responses within a larger amplitude range and temporal window within the somatosensory L2/3 network in *Fmr1*$^{-/y}$ mice. These results thus replicate the clinical phenotype of trial-by-trial variability of physiologically measured sensory responses, and could provide an explanation for the temporal sensory processing issues in autism [18, 19].

Large trial-by-trial variability in AP onset worsens temporal precision of sensory processing

The aforementioned EPSP alterations suggest that the onset of tactile stimulus-evoked APs would also be more variable from trial to trial in *Fmr1*$^{-/y}$ neurons. Tactile HP stimulation elicited APs in at least some of the stimulus trials in about ~ 25% of the recorded neurons (Fig. 1L; proportion *Fmr1*$^{-/y}$ vs. WT, n.s.). We probed AP onset variability by measuring the latency of the first evoked AP within each trial (Fig. 1M–P). While the mean AP onset latency was not different from WT neurons (Fig. 1O, n.s.), the trial-by-trial variability was significantly increased in *Fmr1*$^{-/y}$ neurons (Fig. 1P, $p < 0.01$). An increased AP onset jitter would further reduce the coordinated and reliable processing of sensory information within neocortical circuits, contributing to the temporal processing issues in autistic individuals [18]. In addition to variable timing, we also found a ~ 2-fold increase in the fraction of stimulus trials evoking APs in the *Fmr1*$^{-/y}$ neuronal population, thereby affecting the number of activated neurons per stimulus (Fig. 1Q–T). We conclude that any given tactile HP stimulus elicits variably timed AP firing in approximately twice as many L2/3 pyramidal neurons within the S1-HP region in *Fmr1*$^{-/y}$ mice.

The level of endogenous neural noise correlates with trial-by-trial variability

Endogenous noise [21, 22, 35] at the level of individual neurons or small neural networks has been theorized to be at the root of the variable and unreliable neural sensory processing in ASD [13, 16, 23, 24]. Our high-resolution experimental data in mice (as compared to low-resolution non-invasive human measures) enables us to directly test the validity of this hypothesis [23]. We thus probed changes in the fluctuation of the membrane potential (V_m variance) as key indicator of endogenous noise ([24]; Fig. 2A and B). To better assess the impact of this noise source on sensory processing, we calculated V_m variance just before the arrival of the HP-stimulus evoked response. This baseline V_m variance was on average ~ 2-fold larger in *Fmr1*$^{-/y}$ neurons (Fig. 2B and C, $p < 0.05$), supporting the high-noise model of autism [16]. If this element of endogenous noise could be the cause of the trial-by-trial variability of sensory responses, then it should similarly vary from trial to trial in a correlated manner. We confirmed this prediction by demonstrating a

significantly greater trial-by-trial variability of V_m variance (SD of V_m variance) in *Fmr1*$^{-/y}$ neurons (Fig. 2D and E, $p < 0.05$). Importantly, the magnitude of V_m variance strongly correlated with both the EPSP amplitude and EPSP half-width on a trial-by-trial basis (Fig. 2F; see also V_m variance and EPSP amplitude for same trials, Figs. 2D and 1C).

These results implicate endogenous neural noise as a crucial factor of variable sensory processing in *Fmr1*$^{-/y}$ neurons. The large trial-by-trial variability of endogenous noise levels results in fluctuating functional neocortical states with ensuing consequences for incoming sensory inputs.

Increased trial-by-trial variability of oscillatory power implicating altered synaptic inputs

We then explored the network components of endogenous noise and their impact on sensory processing. Network oscillations resulting from structured synaptic input patterns reflect processes linked to information transfer, perception, cognition, and behavior [36, 37], and dysfunction in these oscillations has been strongly implicated in ASD, serving as physiological biomarker of altered brain states [38]. We probed whether we can detect alterations in the power of the *Fmr1*$^{-/y}$–S1 network oscillations in our single-neuron recordings. We analyzed the spectral power of single-neuron V_m fluctuations for the commonly used frequency bands: delta (1–4 Hz), theta (4–8 Hz), alpha (8–12 Hz), beta (12–30 Hz), and gamma (30–100 Hz) (Fig. 2G–I). This analysis revealed that the power-spectral density (PSD) for these frequency bands was increased in *Fmr1*$^{-/y}$ compared to WT neurons (Fig. 2H–I).

Since periodic activity strongly contributes to the V_m variance and thus endogenous noise, we predicted that the PSD value over this frequency range would similarly vary on a trial-by-trial basis during the baseline phase just prior to the incoming sensory response. Indeed, the baseline PSD value significantly correlated with both the EPSP amplitude and duration on a trial-by-trial basis (Fig. 2F and J). Our data show that dysfunction in oscillatory synaptic input patterns provide an important endogenous noise source for unreliable sensory processing. These results also suggest that measures of oscillation power in clinical studies could be used to predict endogenous neural noise and trial-by-trial variability in neocortical processing in autism.

Greater variability in driving force and elevated spontaneous activity in Fmr1$^{-/y}$ neurons

Neocortical states transition between quieter, hyperpolarized down–states, and more active, depolarized up–states [39] that are characterized by the presence of synaptic input patterns with high-frequency oscillatory components (Fig. 2G). Sensory responses evoked during either an up– or a down–state will be shaped by differences in driving force [40]. In line with our findings of increased trial-by-trial sensory response variability, our fine-scale analysis of the neocortical state transitions revealed that up-states were often fractionated by brief “micro”-up-states (100–150 ms) in *Fmr1*$^{-/y}$ neurons (Fig. 2K and L). The presence of micro up–states (Fig. 2M, $p < 0.01$) was coupled with an overall increase in the up-state frequency (Fig. 2N, $p < 0.01$), and accompanied by a reduced duration and increased frequency of down–

states (Table S1; $p < 0.01$ for both). The greater dynamicity of state transitions also resulted in a broader distribution of up–state V_m values in *Fmr1*$^{-/y}$ neurons (Fig. 2O). Moreover, the up–down–state V_m difference was significantly larger for *Fmr1*$^{-/y}$ neurons (Fig. 2P, $p < 0.05$). Altogether, these alterations would create a broader range of driving forces for incoming sensory responses, in turn enlarging the range of EPSP amplitudes (Fig. 1G). Our data suggests that the increased up–down–state V_m difference and up–state V_m range present crucial endogenous noise features driving increased sensory response variability in *Fmr1*$^{-/y}$ neurons.

In S1, action potentials (APs) are preferentially evoked during up–states, and spontaneous AP activity strongly impacts on sensory information processing (reviewed in [41]). A significant change in this feature might thus indicate a background noise element of the S1 circuitry, altering its operation [21, 42]. We found that a larger fraction of the *Fmr1*$^{-/y}$ neuronal population was spontaneously active (Fig. 3A, n = 4/16 WT and 8/17 *Fmr1*$^{-/y}$ neurons, $p < 0.01$). In addition, while spontaneous AP activity in WT neurons was characteristically low [43, 44] (~ 0.005 Hz), *Fmr1*$^{-/y}$ neurons exhibited a significantly increased spontaneous AP frequency (Fig. 3B and C, $p < 0.05$). These findings suggest a more active basal S1 network state in *Fmr1*$^{-/y}$ mice.

L2/3 pyramidal neurons are more excitable in Fmr1$^{-/y}$ mice

We next explored the contributory role of altered intrinsic excitability in driving endogenous noise. Our data revealed that the number of APs and the maximum AP frequency generated by depolarizing current steps were significantly increased in *Fmr1*$^{-/y}$ S1–HP neurons (Fig. 3D and E, $p < 0.05$), demonstrating that they are intrinsically more excitable. In addition, the APs were wider (Fig. 3F and G, $p < 0.05$) and the after-depolarization (ADP) amplitude of the membrane potential following brief high-frequency bursts of APs was increased (Fig. 3H, $p < 0.05$). The former feature suggests an increased likelihood of AP-evoked transmitter release at the neuron's axon terminals [45, 46], whereas the latter suggests a dendritic hyperexcitability phenotype [46, 47], both acting together to amplify the input–output function of these neurons and ultimately the spread of excitation within the neocortex. Altered excitability might also contribute to the endogenous cellular and circuit noise of S1 by elevating the spontaneous AP firing and increasing the E/I ratio within S1 [13], thus rendering sensory information processing less reliable. Other intrinsic properties, such as resting membrane potential, rheobase, and AP threshold, remained unaltered (Table S1).

Exaggerated variability of numerous features across the Fmr1$^{-/y}$ neuron population

Noisy sensory processing in autistic individuals is characterized not only by increased trial-by-trial variability, but also by greater inter-individual variability [48]. We tested changes in the variability across our neuronal population as a readout for variability in the *Fmr1*$^{-/y}$ population. We compared the variability of both noise- and sensory response related parameters. This analysis demonstrates that the variance of sensory stimulus evoked EPSP (e.g. EPSP half-width, Fig. 3I, $p < 0.05$) and AP (e.g. AP number, Fig. 3J, p <

0.001) responses was higher for the *Fmr1*$^{-/y}$ population than that for the WT population. In addition, variance was also increased for a number of core noise features, including V_m variance (variance of V_m variance, Fig. 3K, $p < 0.01$), oscillation power (e.g. gamma band power, Fig. 3L, $p < 0.05$), spontaneous AP firing (Fig. 3M, $p < 0.001$), and intrinsic excitability (see Table S1 for complete list). These results suggest the presence of a greater range of functional S1 network states within the *Fmr1*$^{-/y}$ mouse population. Additionally, our findings strongly support the idea of elevated inter-individual variability as a hallmark of altered sensory neocortical processing in this preclinical model of ASD.

Broader tuning of S1 neurons suggests reorganization of connectivity

Noisy neural circuits impact on the precision of sensory processing and, together with anatomical-functional alterations, affect the connectivity of neocortical neurons—changes in which have been described in both individuals with autism and ASD mouse models [48, 49, 50, 51]. We tested the relevance of these changes for the specificity of sensory processing, by measuring the receptive field properties of layer 2/3 pyramidal neurons of S1-HP in *Fmr1*$^{-/y}$ mice. Specifically, we asked whether HP neurons would display a differential responsiveness to tactile forepaw (FP) stimulation (Fig. 3N–P). Our results indicate that the percentage of neurons responding to both HP and FP stimuli shifted from ~ 20% in WT mice to ~ 50% in *Fmr1*$^{-/y}$ mice (Fig. 3P, $p < 0.05$). This finding suggests a broader and less specific tuning of these neurons to tactile stimuli of different sub-modalities.

Relationship between endogenous noise and atypical sensory information processing

To integrate the aforementioned findings into a functional model, we developed a correlation matrix (Fig. 4A, B) and visualized the statistically significant correlations in form of a node graph (Fig. 4C, D). This allows us to evaluate the predictive value of our physiological measures for cellular or network function with potential links to increased variability of cellular responses in autism. This analysis revealed that the most prominent nodes based on their number of significant correlations with other parameters were: V_m variance, up–down–state V_m difference, oscillation power, trial-by-trial variability, and EPSP amplitude.

The main findings from the correlation matrix can be summarized as follows: (i) For both *Fmr1*$^{-/y}$ and WT neurons, the (baseline) V_m variance was positively correlated with EPSP amplitude, measures of trial-by-trial (tbt) variability, and the power of theta- and alpha oscillations, and negatively with SNR. For *Fmr1*$^{-/y}$ neurons, the baseline V_m variance was also positively correlated with the power of delta and gamma oscillations, while this correlation was absent in WT neurons. These findings suggest that V_m variance represents an important driver of sensory response amplitude, and in particular its trial-by-trial variability. (ii) For *Fmr1*$^{-/y}$ neurons, the up–down state V_m difference was positively correlated with the EPSP amplitude, baseline V_m variance, and trial-by-trial measures of baseline V_m variance, PSD, and EPSP amplitude. In contrast, these correlations were not present in WT neurons. (iii) The power of the

oscillatory bands strongly correlated with several parameters belonging to different categories in *Fmr1*$^{-/y}$ neurons compared with WT neurons. In particular, there was a strong positive correlation between the power of several oscillations and trial-by-trial variability measures. In addition, gamma power was positively correlated with spontaneous AP firing, baseline V_m variance, and up–state frequency. (iv) For *Fmr1*$^{-/y}$ neurons, the spontaneous AP activity positively correlated with the beta and gamma powers. (v) For *Fmr1*$^{-/y}$ neurons, the maximal AP firing rate (intrinsic excitability measure) was positively correlated with the EPSP half-width and peak latency, and negatively correlated with the beta power. The 3rd AP half-width was positively correlated with the EPSP onset latency and trial-by-trial EPSP half-width.

Altogether, for the *Fmr1*$^{-/y}$ neuronal population many more parameters correlated positively with each other when compared to the WT neurons. Among these parameters, the strongest correlations were found between endogenous noise sources, variability measures and EPSP parameters. V_m variance, up–down state V_m difference, and oscillation power emerge as core endogenous noise parameters that strongly determine atypical sensory information processing in the S1-network. Thus, trial-by-trial variability of sensory responses is largely attributable to the neocortical state at the time of the incoming sensory responses. More specifically, *Fmr1*$^{-/y}$ neurons displaying the strongest HP stimuli-evoked responses are also those exhibiting the largest trial-by-trial variability, V_m variance and up–down state V_m difference. This correlation between the three aspects of information processing is highly pertinent and could point to important physiological biomarkers for clinical studies.

Dissecting the origin of the different endogenous noise sources

We asked whether we could further dissect the origin and functional role of the different components of endogenous noise in *Fmr1*$^{-/y}$ neurons. To address this, we pharmacologically targeted the voltage-, and calcium-sensitive K^+ channel, BK_{Ca} channel, an approach that has previously been shown to correct cellular hyper-excitability [45, 46, 52, 53]. To test whether the endogenous noise elements arise locally at the level of the S1, we developed an *in vivo* neocortical assay in which we applied the BK_{Ca} channel agonist locally to the S1 surface (Fig. 5A). This strategy was enabled by employing the highly selective $BK_{Ca,}$ agonist, BMS191011 [54], which has poor penetration in complex tissue such as the brain due to its binding to protein and other complex biomolecules. Our strategy allowed us to distinguish cellular and network deficits that were sensitive to local manipulation of BK_{Ca} channels from those that were not affected.

This analysis revealed that many features of HP stimulus evoked EPSPs, including the mean amplitude, half-width, rise slope, and onset latency, were corrected by BMS191011 application (Fig. 5B–F, WT vs. *Fmr1*$^{-/y}$-BMS191011, normalized data, see methods; all n.s.). In addition, alterations related to certain endogenous noise features, such as spontaneous AP firing (AP firing rate, Fig. 5G; percentage of spontaneously active cells, Table S1) and intrinsic excitability (AP half-width, Fig. 5H and I; ADP amplitude, Table S1) were corrected (all n.s.).

Moreover, BMS191011 significantly diminished the inter-neuronal variability of several features related to sensory responses (e.g. EPSP amplitude, Fig. 5J, $p < 0.05$; EPSP half-width, Fig. 5K, n.s.; EPSP onset latency, Table S1, n.s.) as well as that of spontaneous AP firing rate (Fig. 5L, n.s.) across the *Fmr1*$^{-/y}$ neuron population.

All these corrections could be explained by the role of BK_{Ca} channels in regulating dendritic excitability as well as AP properties in the axons and axonal terminals locally within S1, which in turn determines the accompanying calcium influx and transmitter release probability.

In contrast, trial-by-trial variability of EPSP amplitude (Fig. 5M, $p < 0.01$) and half-width (Fig. 5N, $p < 0.05$) was not affected by local BMS191011 application in *Fmr1*$^{-/y}$ neurons. Accordingly, BMS191011 treatment also had little or no effect on those core components of endogenous noise that strongly correlated with trial-by-trial variability of EPSP amplitude: baseline V_m variance (Fig. 5O and P, $p < 0.05$), up–down–state V_m difference (Fig. 5Q, $p < 0.01$), and the power of oscillations (Table S1).

Collectively, our results show that localized BMS191011 application reduces elevated spontaneous AP firing as well as neuronal excitability, dampens the impact of HP-stimulus evoked responses, and reduces inter-neuronal variability in S1–*Fmr1*$^{-/y}$–L2/3 pyramidal neurons. However, BMS191011 application within S1 did not correct the trial-by-trial variability of EPSPs, nor the endogenous noise sources that strongly relate to this feature, such as the power of periodic synaptic input patterns, up–down–state V_m difference and V_m variance.

Our results provide evidence for the usefulness of mechanism-based targeted approaches for the dissection of the different noise sources, and the examination of their relationship with atypical sensory processing features.

Discussion

These results demonstrate that the complex variability features of sensory processing are recapitulated with surprising fidelity in a preclinical mouse model of autism. Crucially, we discovered core endogenous noise elements that drive elevated response variability. These results suggest that this elevated response variability has both cellular and network origins. Our work thus provides a framework for understanding the role of endogenous noise in atypical sensory information processing in autism. With this in mind, we developed a model integrating the principal sources and features of altered endogenous neural noise and their contribution to atypical variability and unreliability of sensory information processing in ASD (Fig. 6).

We propose that changes in network-level synaptic inputs (synaptic noise) impinging on S1–*Fmr1*$^{-/y}$–L2/3 pyramidal neurons together with dysfunction in their intrinsic excitability (ion channel noise) give rise to elevated endogenous noise. At the single-cell level, this endogenous noise is expressed as alterations in the oscillatory power, up–down–state difference, and variance of the membrane potential,

as well as an elevated level of spontaneous AP firing as core noise components. These features are strongly correlated with the variability of sensory responses, in particular changes in their magnitude and temporal aspects. In addition, these noise components influence each other, further exacerbating their impact on sensory processing. For instance, an increased power in network oscillations and intrinsic excitability strongly contribute to an increase in V_m variance; V_m variance in turn initiates up–down state transitions, which together with the greater up–down–state V_m difference drives a larger range and trial-by-trial variability of EPSP amplitudes. Thus, the presence of fluctuating levels of endogenous noise underlies rapid changes in neocortical functional connectivity by creating an unstable S1 circuitry.

These unstable functional S1 states could explain many different aspects of the complex and nuanced symptomatology of sensory features in autism. This includes issues with temporal processing, hyper– and/or hypo–sensitivity to sensory stimuli, multisensory binding, and impaired predictive abilities. Importantly, our findings could explain the greater trial–by–trial and inter-individual variability of sensory responses observed in autistic individuals. Our data also provide the first experimental evidence addressing the question whether endogenous noise is increased or decreased in small-scale networks in autism. Moreover, our model points to a set of translational biomarkers which are predictive of endogenous noise and can be measured in autistic individuals (Fig. 6; see also ‘biomarkers’, below).

Alterations in spontaneous activity suggest a more active and unstable neocortical network state

Spontaneous AP activity in the neocortex contributes to the dynamicity of the network state, interacting with the processing of incoming sensory information [21, 42], and enabling adaptive behavior [55]. An elevated level of spontaneous AP activity may impact the capacity to correctly predict, perceive, and interpret incoming information (reviewed in [8, 41]). Our finding of increased spontaneous AP activity of S1–L2/3 neurons in *Fmr1*$^{-/y}$ mice is consistent with previous findings in both awake and anesthetized mice [56]. Additionally, we found that a larger fraction of the *Fmr1*$^{-/y}$–L2/3 population was spontaneously active, suggesting an overall augmented background noise of the S1 network in *Fmr1*$^{-/y}$ mice. This increased background noise will influence the rhythmicity of network oscillations and contribute to the increased V_m variance observed in *Fmr1*$^{-/y}$–S1 neurons with ensuing functional consequences for sensory information processing, as shown by our correlation analysis (Figs. 4 and 6).

Up–down–state levels create more diversity in driving force for synaptic responses

Neocortical states are characterized by periodic up–/down–state transitions occurring during quiet rest, sleep, and anesthesia, as well as when animals perform perceptual tasks, and influence the responses of somatosensory neurons to subsequent sensory stimulation (reviewed in [57]). Up–states are associated with a marked increase in local neocortical network activity and in the power of higher-frequency component oscillations (including gamma, Fig. 2G) [58]. The heightened dynamicity of up–down–state

transitions in S1-*Fmr1*$^{-/y}$ neurons could contribute to the clinically observed variability in sensory evoked responses. In addition, the greater range of up–down–state V_m difference is expected to result in a larger range of response magnitudes due to larger differences in the driving force. These dynamic network state changes could conceivably contribute to heterogeneity in sensory features in autism, namely hyper- and hyposensitivity reported for the same sensory modality.

Dysfunctional oscillatory power reflects deficits in synaptic input patterns

Our data indicate the presence of a higher power of delta, theta, alpha, beta, and gamma oscillations in *Fmr1*$^{-/y}$ neurons. Due to their contribution to endogenous neural noise and thereby sensory information processing (Figs. 4 and 6), dysfunction in these oscillations suggests changes in processes linked to information transfer, perception, cognition, and behavior [36, 37]. Notably, the augmentation in gamma power might relate to the aforementioned increase in spontaneous AP firing in *Fmr1*$^{-/y}$ neurons (Fig. 4B, D; [32, 59]), and reflect increased neocortical network excitation and altered E/I ratio [60]. Elevated broadband gamma noise is also associated with reduced spike precision and ability to synchronize periodic gamma band activity, and social and sensory processing difficulties, and may have cascading effects on cognitive, behavioral, and neuropsychiatric symptoms [61, 62]. Our findings of a wide range of gamma power values among the *Fmr1*$^{-/y}$ neuronal population suggests that there might be subgroups of individuals based on the presence of higher and lower gamma power levels [63]. A link between increased gamma power and L2/3 network hyperexcitability has also been described *ex vivo* for the auditory cortex [64]. Mechanistic insight into abnormal gamma power from single-neuron recordings may have ramifications for better understanding the pathophysiology of sensory symptoms in autism.

Consequences of noise for stimulus-evoked tactile sensory processing in ASD

Our findings suggest that key parameters of endogenous neural noise, especially V_m variance, up–down–state V_m, and oscillatory power, are altered, crucially impacting the magnitude, temporal resolution, and variability/reliability of tactile sensory responses within the L2/3 network of *Fmr1*$^{-/y}$ mice (Figs. 4 and 6). Indeed, we find that the onset of EPSPs following hind-paw stimulation is faster, their amplitude and rise slope increased, and their duration prolonged. Tactile stimulation also evokes more variably timed APs and a greater number of APs within the L2/3 network which, together with broadening of APs, increases the probability of spreading this information to postsynaptic targets. Increased noise, however, also reduces the reliability of sensory responses through its contribution to greater trial-by-trial variability. Augmentation of sensory responses along with greater variability across trials results in a larger repertoire of potential response features, including a larger amplitude range and wider temporal integration window, and APs that are consequently evoked at very different time points. This larger dynamic range strongly correlates with endogenous noise, which shows an overall increase but also significant variability on a trial-by-trial basis. An optimal endogenous noise level could be beneficial [65, 66],

improving neuronal responsiveness and thus perceptual detection sensitivity, whereas higher noise levels would randomize neuronal responses and impair behavioral performance [67]. Together, these variable network states have the potential to explain both superior and inferior sensory detection and discrimination skills, sensory hypersensitivity, hyposensitivity, and temporal processing issues in autism [6, 12, 15, 18, 19, 68, 69]. In a hyper-excited state, the network's computational property of divisive normalization is degraded and its E/I ratio is enhanced [13, 70, 71]. Our work suggests a complex scenario in which more variable (and thus unpredictable) neocortical sensory responses form part of the neurophysiological signature of autism.

In human studies, the consequences of noise present as increased variability in the magnitude and dynamics of evoked neuronal responses to sensory stimuli [7, 8, 11, 12]. We find it intriguing and highly pertinent that these hallmarks of atypical sensory responses, measured in clinical studies at the scale of large neuronal networks (fMRI, EEG, or even behavioral responses) are recapitulated by our single-cell measures in a preclinical model. These parallels between neural measures reflecting small scale networks and human physiological responses suggest that it is possible to exploit our findings to dissect the mechanisms underlying complex clinical measures.

Lastly, our data demonstrate a higher prevalence of tactile *forepaw* stimulus-related responses in L2/3 pyramidal neurons of the S1 *hindpaw* region, indicating reorganization of the structural or functional connectivity of the sensory cortex (for similar findings in the visual cortex, see [49]). Functionally, this results in changes in the receptive field properties of L2/3 pyramidal neurons of S1–HP. Similar findings have been described for L2/3 pyramidal neurons of the whisker-related S1 barrel cortex [72] and auditory cortex [73]. Changes in synaptic connectivity would add noise to the network, leading to compound changes in neuronal computation with negative consequences for sensory filtering or transmission of information to associative sensory areas, and potentially behavioral or perceptual responses, as suggested by Cascio et al. [74]. Functional connectivity re-organization, along with enhanced stochastic resonance are also proposed neural mechanisms of synesthesia, which commonly occurs in ASD [14, 75]. Together with the increased probability of neurotransmitter release due to broadened APs [45], the increased level of sensory stimulus-evoked APs and connectivity reorganization provide a multiplicative noise source by more efficiently spreading information to a larger postsynaptic network.

Biomarkers

A major challenge to sensory-based autism research is the development of optimized biomarkers that allow direct comparisons between rodents and human subjects while simultaneously permitting exploration of the underlying neurobiological mechanisms. Based on our analysis of noise sources, we have identified several measures (Fig. 6) that are highly translatable between preclinical and clinical settings. Although these measures were obtained here using single-cell recordings in rodents, equivalent measures can be obtained by large-scale electroencephalography (EEG) or psychophysical methods in humans.

Our analysis of single neocortical neurons in *Fmr1*$^{-/y}$ mice suggests a change in basal oscillatory power over a range of frequencies. Notably, these measures strongly correlate with other sources of endogenous noise, particularly V_m variance, up–down state V_m difference, and spontaneous AP firing. Here, the power of delta, theta, gamma, and, to some extent, alpha oscillations also correlates with measures of trial–by–trial variability for sensory evoked responses. Although a relationship between changes in gamma (30–80 Hz) power and sensory issues has been suggested in human studies (reviewed in [61, 76]), a specific relationship with trial-by-trial variability has not yet been established and merits further exploration. Interestingly, our correlation analysis suggests a strong relationship between gamma power and other noise sources as well as atypical sensory responses. This cross-species conservation of resting–state gamma power changes is remarkable, suggesting its potential as a useful marker of endogenous noise.

Neocortical evoked responses can be measured in humans using EEG, magnetoencephalography (MEG), and/or fMRI in combination with tactile stimuli (e.g., clothing, air puffs, or naturalistic vibrotactile stimulation) applied to the hand, fingertips, or arm. In general, such studies report that neocortical responses are atypical in autism. Notably, these physiological measures are also highly predictive when associated with clinical measures of symptom severity or questionnaire-based sensory profiles (e.g., [74, 77, 78, 79, 80]). However, questions remain regarding their capacity to reveal mechanisms underlying atypical endogenous noise [24]. Our results (Fig. 6) suggest a strong correlation between endogenous noise parameters and both the magnitude, temporal features, and variability of sensory evoked responses, as well as measures of trial-by-trial variability.

Testing the origin of noise sources by targeting local neocortical ion channel dysfunction

By targeting a relevant cellular mechanism locally within S1, we gained further insight into the underpinnings of endogenous noise and atypical sensory processing, and the spatial origin of those changes (i.e. generated within or outside of S1). We chose to target BK_{Ca} channels because of their role in regulating AP features, neurotransmitter release probability, and dendritic excitability — features that likely contribute to some of the measured endogenous noise sources and sensory response alterations. In addition, these channels have previously been implicated in autism [52] and sensory information processing [53] and suggested as suitable targets for intervention [45, 46, 81, 82].

Our data show that local neocortical application of the selective BK_{Ca} agonist, BMS191011, can correct AP half-width and ADP, reduce spontaneous AP firing, and restore multiple aspects of tactile information processing in S1–HP L2/3 pyramidal neurons including the EPSP amplitude and half-width and their inter-neuronal variability. This finding of a localized pharmacological intervention effect supports the idea that some of the neurobiological alterations of atypical sensory information processing in autism arise at the level of S1 and are related to BK_{Ca} channel dysfunction.

On the other hand, local BK_{Ca} channel modulation had no significant impact on key endogenous noise measures correlating with the trial-by-trial variability of EPSP amplitude and half-width, namely V_m

variance, up–down–state V_m difference and oscillatory power. Thus, endogenous noise features that drive trial–by–trial variability either originate outside of the S1 network such as synaptic noise arising from long-ranging connections, are insensitive to BK_{Ca} channel agonists, or require a more global application of BK_{Ca} channel agonists. Our framework allows the evaluation of local or global manipulation on endogenous noise sources contributing to atypical sensory information processing in autism.

Positioning our findings in the context of signal detection theory

Neural sensory information processing consists of a stimulus-specific component and noise. Based on signal detection theory, the relationship among signal, noise, and neural output in the sensory cortices can be expressed using the following mathematically defined model [15, 20, 83]: $O = K(S) \times (1 + N_m) + N_a$. Here, the neuronal output (O) is a function of the encoding function of the signal (K), the signal itself (S), and various noise sources, namely, multiplicative noise (N_m; stimulus related) and additive noise (N_a; stimulus independent). N_m, for example would cause the signal to spread more widely within the network, in line with computational motifs such as reduced divisive normalization, enhanced E/I ratio model and the “intense world theory” [13, 84, 85, 86]. While it is important to note that it may be difficult to discriminate between multiplicative noise, gain control and additive noise, our experimental findings provide a starting point in this direction. In particular, our data reveal atypical features in the *Fmr1*$^{-/y}$ neurons that would suggest both K(S), N_m, and N_a alterations. The endogenous noise parameters described in our study (V_m variance, up–down–state V_m difference, spontaneous AP firing, and network oscillation power) would be crucial contributors of additive noise. In addition, these measures would also affect the gain or encoding function (altered synaptic summation and AP output). An increase in neuronal excitability would contribute to the additive noise, a modification of the gain function (enhanced neural throughput), and multiplicative noise (enhanced spread of the signal to postsynaptic targets due to increased transmitter release probability). The alterations in the receptive field properties observed in *Fmr1*$^{-/y}$ neurons are indicative of an enhanced functional–structural connectivity, which would strongly affect N_m. The functional outcome of the combined changes would vary on a trial–by–trial basis and depend strongly on the highly fluctuating endogenous noise levels with ensuing consequences for sensory processing. Given the strong correlation between atypical sensory symptoms and autism severity, future studies encompassing measures of cellular/network noise are warranted (Fig. 6). To this end, our study points to a number of biomarkers that are likely to be useful indicators of noise. Understanding the role of noise in sensory information processing may lead to new interventional strategies, whether behavioral, environmental, or pharmacological, to relieve the stress and conflict that these experiences generate.

Materials And Methods

Experimental Design

We performed *in vivo* whole–cell patch–clamp recordings of neocortical neurons of the primary somatosensory cortex to examine tactile stimulus–evoked sensory processing in anesthetized mice and to probe the causal role of endogenous noise sources and parameters for atypical sensory information processing in autism. Throughout the text, the terms autism and autistic people/individuals are used, in line with recent evidence suggesting that these terms are preferred in the autistic community and are less stigmatizing [87].

Ethical statement

All experimental procedures were performed in accordance with the EU directive 2010/63/EU and French law following procedures approved by the Bordeaux Ethics Committee (CE2A50) and Ministry for Higher Education and Research. Mice were maintained under controlled conditions (temperature 22-24°C, humidity 40-60%, 12h/12h light/dark cycle, light on at 07:00) in a conventional animal facility with *ad libitum* access to food and water. All experiments were performed during the light cycle.

Mice

Second generation *Fmr1* knockout (*Fmr1*$^{-/y}$) [46] and wild-type littermate mice at P26-42 were used in our study. Mice were maintained in a mixed 129/Sv/C57Bl/6J/FVB background (backcrossed 6 generations into C57Bl/6J) as described in [46]. Male wildtype and *Fmr1*$^{-/y}$ littermates were generated by crossing *Fmr1*$^{+/-}$ females with *Fmr1*$^{+/y}$ male mice from the same production, and the resulting progeny used for our experiments was either *Fmr1*$^{+/y}$ (wild-type) or *Fmr1*$^{-/y}$ (KO). Mice were maintained in collective cages following weaning (3–5 litter males per cage). Cages were balanced for genotype and supplemented with minimal enrichment (cotton nestlets). Number of mice are given in the figure captions. The genotype of experimental animals was re-confirmed *post-hoc* by tail-PCR.

Surgery

Mice (P26–42) were anaesthetized with a mixture of ketamine (100 mg.kg^{-1}) and xylazine (10 mg.kg^{-1}) injected intraperitoneally and supplemented as necessary throughout the procedure. Proper depth of anesthesia was monitored by testing the absence of a foot-pinch reflex and whisker movement. Mice were head-fixed using non-puncture ear-bars and a nose-clamp (SR-6M, Narishige). Body temperature was maintained at 37°C. Prior to making an incision on the skin to expose the skull, 0.1 ml of a 1:4 Lidocaine to saline solution was administered subcutaneously and waited for 2 to 5 minutes to induce local analgesia. Following a careful removal of the scalp, and the remaining tissue on the skull, a small craniotomy was made above the S1 hindpaw region (1 mm posterior and 1.5 mm lateral from Bregma, confirmed with intrinsic imaging coupled with hind paw stimulation) using a dental drill (World Precision Instruments).

In vivo whole-cell patch-clamp recordings

Blind, *in vivo* whole-cell recordings were performed from layer 2/3 pyramidal neurons of the hindpaw region of S1 in anaesthetized mice, as described previously [44, 46]. Neurons were identified by their

electrophysiological properties, and in some cases by their *post-hoc* morphology. Depth of neurons was on average 263 µm from pia, ranging from 175 µm to 374 µm. There was no genotype difference in the depth of recording (WT = 261.69 ± 34.91 µm; *Fmr1*$^{-/y}$ = 259.72 ± 49.12 µm; $p > 0.05$, unpaired student t-test). Data were acquired at 20 kHz sampling rate and low-pass filtered at 3 kHz using Dagan BVC-700A amplifier (Dagan, Minneapolis, USA), Digidata 1320A and Clampex 10.4 software (Axon Instruments). Recording pipettes with an open-tip resistance of 4–6 MΩ were pulled from borosilicate glass using a PC-10 puller (Narishige) and filled with intracellular solution containing (in mM): 130 K-methanesulphonate, 10 Hepes, 7 KCl, 0.05 EGTA, 2 Na_2ATP, 2 MgATP, 0.5 Na_2GTP (all products from Sigma Aldrich); pH 7.28 (adjusted with KOH); osmolarity was 280–295 osm. In a subset of experiments, biocytin (1.5–2.5 mg/ml) was added to the recording solution for post-hoc neuronal identification and anatomical comparison. The intracellular solution was filtered using a 0.22-µm pore-size centrifuge filter (Costar Spin-X). Cells were excluded from the analysis if the pipette access resistance exceeded 50 MΩ or the neuron was depolarized more than − 50 mV.

Neocortical application of the specific BK_{Ca} channel agonist, BMS191011

To pharmacologically target BK_{Ca} channels, we used the specific channel agonist, BMS191011 (3-[(5-Chloro-2-hydroxyphenyl)methyl]-5-[4-(trifluoromethyl)phenyl]-1,3,4-oxadiazol-2(3*H*)-one, 100 µM; Tocris). A stock solution with a concentration of 50 mM BMS191011 was prepared in DMSO and stored at − 20°C. For direct neocortical application the drug was diluted to a final concentration of 100 µM in PBS (final concentration of DMSO in PBS: 0.2%). Cortical application of BMS191011 (~ 1 ml) was performed at least 30 minutes prior to the whole-cell patch-clamp experiments. Drug allocation was semi-randomized and balanced for cage composition.

Data analysis

Neuronal morphology

Following biocytin (1.5–2.5 mg/ml Biocytin, Sigma) filling of the neurons during recording, mice were perfused for *post-hoc* staining [46]. Briefly, mice received a lethal dose of pentobarbital (300 mg/kg, *i.p.)* delivered in the presence of lurocaine (30 mg/kg; i.p.). Following respiratory arrest (and after verifying the absence of reflexes to toe/tail pinch and eye-blink) tissue was fixed by trans-cardial perfusion with 1 X PBS (pH 7.4), followed by 4% paraformaldehyde in 1 X PBS (pH 7.4). Brains were then post-fixed for 2h in 4% PFA (or stored in 1 X PBS prior to slicing). Subsequently, 80-µm-thick slices were cut using a vibratome (Leica), and the slices were stored in 1 X PBS prior to staining. Biocytin was revealed using streptavidin-Alexa Fluor 555 (Invitrogen). Slices were mounted in Mowiol and neuronal morphology was reconstructed using a Neurolucida system (MBF Biosciences) equipped with a 100x oil immersion objective lens.

Spontaneous AP firing

Neurons that spontaneously fired at least one action potential (AP) during a 120-second-time window were considered spontaneously active, otherwise silent. Spontaneous AP rate was calculated as the number of APs elicited during this 120-second-time window. The analysis included data from both active and silent neurons. We acknowledge the limitation of the term ‘silent’, since these neurons would likely become ‘active’ if we would analyze spontaneous AP firing over a longer time window. As a result, many WT neurons had spontaneous AP firing values of zero and we could therefore not include this feature in our correlation matrix and the accompanying node plot for WT neurons.

Up– and down–states

For up– and down–states, both ‘active and silent cells’ were included in this analysis. Custom-made python scripts were used to detect all up– and down–states during a 180-second recording period, and to quantify their duration, frequency, and membrane potential at the respective states. A pre-processing step was performed when necessary to correct for linear drifts in membrane potential. Our algorithm annotated each point of the signal as either an up– or down–state with no intermediate state. A gliding threshold was calculated every second as the median of all points during both a four-seconds-period before and after that point. For each point of the signal the median of the surrounding points (during 50 ms before and after) was computed and compared to the corresponding gliding threshold. If this median was greater than this threshold, the point was considered part of an up-state and vice versa. Our analysis revealed “micro”-up-states lasting between 100 and 150 ms. Events lasting less than 100 ms were considered too short and removed from the analysis.

Power of membrane potential oscillations

The two periodograms (WT and KO) were obtained utilizing the Welch function of the Python open-source library, SciPy. Parameters such as a 4-second Hann sliding window, a 50% overlap and the mean periodogram as the averaging method were used to calculate the Power spectral density (PSD). PSD values for each delta (0.5–4 Hz), theta (4–7 Hz), alpha (8–12 Hz), beta (13–30 Hz), and gamma (30–100 Hz) bands were computed by calculating the area under the curve of the periodogram to the respective frequency band by applying the composite Simpson rule.

Membrane potential fluctuations/wavelet analysis

Spontaneous resting signals were transformed using a complex Morlet wavelet with 4Hz as mother wavelet frequency [38]. The widths used to scale the wavelets were computed using the following equation:

$$\frac{(w * Fs)}{(2 * yScale)}$$

where w is the mother wavelet frequency, Fs the sampling rate (20kHz), and yScale is scale of the frequencies we are interested in. Absolute values were plotted in color-code with the scale ranging from 0

to 3. This maximum is a tradeoff between being able to detect the differences between genotypes but not saturating the signal.

Intrinsic properties

To study the intrinsic properties of the recorded neurons, we measured the membrane potential responses to 500-ms long step current injections ranging from – 450 pA to 550 pA (step size: 50 pA). To determine the action potential (AP) threshold, we measured the membrane potential where the slope of its rising phase exceeded 10 mV/ms. AP half-width was determined by measuring the duration of the first AP at half maximal amplitude (half-distance from threshold to peak) following the rheobase injection. Maximum AP frequency was calculated from the voltage trace with the largest number of APs. Calculation of AP accommodation was performed using a voltage trace encompassing 5 APs. Briefly, the spike interval (SI, in ms) between the 1st and 2nd AP (1st spike interval, SI), and the 4th and 5th AP (4th SI) were calculated, and AP accommodation was then calculated as 4th SI/1st SI. For analysis of the AP after-depolarization (ADP), trains of three APs at various frequencies were generated by brief somatic current injections (1 nA, 1.08 ms). Only AP trains occurring during down–states were selected for the analysis. Three to six trials were averaged, and the ADP amplitude (from baseline) was measured 5 ms after the peak of the last AP. AP half-width ratio was measured as the ratio of the third and first AP. To measure input resistance, we injected 500-ms-long hyperpolarizing (-100 pA) current pulses and measured the steady-state membrane potential deflection at 300 ms relative to baseline.

Sensory stimulus evoked responses - Hindpaw (HP) and forepaw (FP) stimulation

Sensory responses to tactile paw stimulus were evoked by applying squared current pulses (2 ms duration, 100 V, 30 mA) to the paws via conductive adhesive strips (~ 1 cm^2) placed on top of, and underneath the HP or FP, as described previously [44, 46]. These conductive strips covered the entire paw. Following the establishment of a somatic whole-cell recording configuration, the contralateral HP or FP was stimulated 40 times at an interval of < 0.3 Hz.

EPSPs and signal-to-noise (SNR) ratios

Parameters of HP stimulus evoked excitatory postsynaptic potentials (EPSPs) from 40 successive trials were calculated for EPSP-only neurons (neurons responding to HP stimulus exclusively in a sub-threshold manner, i.e. an EPSP or a failure) using Clampfit software (version 11.1, Molecular devices, LLC). Briefly, the maximum EPSP amplitude was determined for each trial during a 200-ms time window following the HP stimulation. Trials with a response amplitude of less than two times the standard deviation of the baseline were considered as failures. EPSP duration was calculated by measuring the width of the response at half-maximal amplitude. Response slope was estimated as the rise slope between the 20th and 80th percentile of the EPSP amplitude relative to the baseline. Baseline membrane potential (V_m) fluctuation was calculated as the standard deviation (SD) of the V_m fluctuation during a 200-ms-time window just before the stimulus onset. Signal-to-noise ratio (SNR) was calculated similar as described in

Dinstein et al. [6], by dividing the EPSP amplitude of each trial by the EPSP amplitude variance across trials for each cell. EPSP latencies were measured for the averaged response for each cell. EPSP onset latency was measured as the delay following HP stimulation where the Gaussian fit of the response's rising phase crosses the V_m baseline (averaged V_m potential during 200 ms before stimulus onset). Peak latency was calculated as the delay of the EPSP maximum amplitude with respect to the onset of the response.

Evoked APs

Neurons were included in the evoked AP analysis if HP stimuli elicited at least one AP during the 40 trials. Accordingly, these neurons were classified as AP-EPSP neurons. The quantification of evoked AP responses was adapted from [44, 46]. Briefly, spontaneous AP firing (pre-stimulus APs) was calculated as the number of APs elicited within a 200-ms-time window prior to HP stimulus. The evoked AP firing was quantified as the difference between the number of APs fired within a 200-ms-long time window following the HP stimulation (post-stimulus APs) and the pre-stimulus AP number (evoked APs = post-stimulus APs – pre-stimulus APs). Coefficient of variation (c.v.) was calculated by dividing the standard deviation of AP firing by the mean evoked AP firing for individual trials. Mean AP number per successful trial was determined by dividing the number of APs evoked during a 40-trial session by the number of trials eliciting at least one AP. To determine AP dispersion, we measured the onset of the first AP in each trial within a 70-ms-time-window following HP stimulus.

Correlation matrix and node plot

The correlation graphs were created with python custom-made script using NetworkX and Netgraph libraries. Seven categories of parameters (in WT neurons six, since spontaneous AP firing could not be included, see above) were defined: Trial-by-trial variability parameters, up–/down–state parameters, spontaneous AP firing, AP parameters, membrane potential (V_m) variance parameters (PSD + SD baseline V_m variance), SNR parameters, and EPSP parameters. Parameters were ordered depending on these categories, and each category is displayed in a different color in the graph. The nodes were arranged on a circular layout and the size of the nodes is proportional to their degrees – in this case the number of statistically significant correlations. Only correlations with a p-value < 0.05 using the Pearson test are shown. Edge size and color depend on the correlation coefficient, larger coefficients (absolute value) have edges with greater width and darker color (blue for negative and red for positive correlations).

Trial correlation parameters

The time window chosen to compute V_m baseline parameters (baseline V_m, baseline V_m SD, PSD) on a trial-by-trial basis was a range of 200 ms before the onset of the HP stimulus. To estimate the influence of baseline V_m fluctuation and PSD on the strength, duration, and reliability of HP stimulus evoked EPSPs, these parameters were normalized by the baseline V_m. For correlating these parameters for each trial, we used Pearson correlation tests.

Data normalization in Fig. 5

To assess whether BMS191011 application corrected the altered physiological features of *Fmr1*$^{-/y}$ neurons, we statistically compared WT and *Fmr1*$^{-/y}$-BMS191011 values after they were both normalized by *Fmr1*$^{-/y}$ values (Fig. 5, panels C, F, G, H, I, M, O, P, Q, S, T). For spontaneous AP firing (panel D) it was not possible to normalize this data because of the high proportion of zero values for WT and *Fmr1*$^{-/y}$-BMS191011 neurons. Values were either normalized by the mean of the *Fmr1*$^{-/y}$ values if these values were normally distributed, or by the median in case of non-normally distributed data. This is stated for each panel in the legend of Fig. 5.

Overall experimental design and analysis

Sample sizes were determined based on our published work [44, 46]. In addition, we performed *posthoc* statistical tests of power. Mice of both genotypes were littermates and randomly assigned. Recordings and analysis were performed blind to the genotype.

Statistical analysis

Values were first tested for outliers (Grubb's outlier test with alpha = 0.05). These outliers were removed from the statistical analysis and the resulting plots. Values were also tested for normality using the Shapiro-Wilk normality test. If the values were normally distributed an unpaired t-test was used to compare two groups. For non-normally distributed parameters we used Mann-Whitney's U-test. A mixed ANOVA model was used for repeated measurements. As we combined silent neurons (no firing in 2 min time window) and active neurons for the calculation of spontaneous properties, we have performed a two-sided non-parametric permutation test to calculate the p-Value. Boxplots indicate the median value (middle line), the mean (green line), as well as the 25th and 75th percentiles (box). The lower whisker will extend to the first datum greater than Q1 – 1.5*IQR where IQR is the interquartile range (Q3-Q1). Similarly, the upper whisker will extend to the last datum less than Q3 + 1.5*IQR (matplotlib boxplot function default parameters). Correlation matrices were made with R Pearson tests, resulting in a coefficient of correlation and an associated p-value. Trial-by-trial variability was calculated as standard deviation of the parameter values across all trials for each cell. The F-test of equality of variances or Bartlett test were used to explore the difference in variance between genotypes at the cell-population level (trial-wise average) for normally distributed data. For non-normally distributed data the Levene test was used with the mean as center parameter. Density plots (Rugg plots) were made with a gaussian kernal density estimation using the function scipy.kde.gaussian_kde from the python library scipy. P values < 0.05 were considered significant (* P < 0.05, ** P < 0.01, *** P < 0.001).

Declarations

Acknowledgments

General:

We would like to thank Drs. M. Brecht, Troy Margrie, and Jérôme Epsztein for help with setting up the in vivo patch-clamp techniques in our laboratory. We thank Dr. Katy Le Corf, Dr. Rémi Proville and Mrs. Sreedevi Madhusudhanan for assisting with analyses and immunohistochemistry. We thank Drs. Ede Rancz, Cyril Herry, Yves LeFeuvre, and Ourania Semelidou for feedback on the manuscript.

Funding:

This project was funded by ENC network-European Erasmus Mundus Joint PhD Fellowship (A.A.B.), Fondation pour la Recherche Médicale PhD extension grant FDT20170437003 (A.A.B.), Fondation pour la Recherche Médicale postdoctoral grant SPF20130526794, ING20140129376 (G.B.), INSERM (A.F.), Marcel Dassault-Fondation FondaMental Award 2019 (A.F.), Simons Foundation Autism Research Initiative (A.F.), and Fondation de France (A.F.).

Author contributions:

A.F. conceived the project. A.F., A.A.B., G.B. designed the experiments. A.A.B., G.B. and Y.V. performed the experiments. A.A.B., T.G., Y.V, and G.B. analyzed the data. T.G. developed python computational codes for some of the analyses. M.G. contributed to the interpretation of the data and logistic support of the study. A.F., A.A.B., T.G. prepared the figures. A.F., M.G., and A.A.B. wrote the manuscript, and T.G., Y.V. provided feedback on the manuscript.

Inclusion and diversity statement:

We support inclusive, diverse, and equitable conduct of research. We tried to use inclusive language as much as possible.

Competing interests:

The authors declare that they have no competing interests.

Data and materials availability:

All data are presented within the main text or in the supplementary materials. Raw data are stored on local servers. Python codes that have been used for the analysis can be available on request after the publication of the manuscript.

References

1. Tomchek SD, Dunn W. Sensory processing in children with and without autism: a comparative study using the short sensory profile. *Am J Occup Ther* **61**, 190-200 (2007).
2. Fernandez-Andres MI, Pastor-Cerezuela G, Sanz-Cervera P, Tarraga-Minguez R. A comparative study of sensory processing in children with and without Autism Spectrum Disorder in the home and classroom environments. *Res Dev Disabil* **38**, 202-212 (2015).

3. Mikkelsen M, Wodka EL, Mostofsky SH, Puts NAJ. Autism spectrum disorder in the scope of tactile processing. *Dev Cogn Neurosci* **29**, 140-150 (2018).
4. American Psychiatric association A. *Diagnostic and statistical manual of mental health disorders* 5th edn. American Psychiatric Publishing (2013).
5. SFARI-Workshop. https://www.sfari.org/2019/03/28/coordinating-animal-and-human-based-research-on-sensory-alterations-in-autism-spectrum-disorders/. In: *SFARI Workshop*) (2018).
6. Dinstein I, Heeger DJ, Lorenzi L, Minshew NJ, Malach R, Behrmann M. Unreliable evoked responses in autism. *Neuron* **75**, 981-991 (2012).
7. Milne E. Increased intra-participant variability in children with autistic spectrum disorders: evidence from single-trial analysis of evoked EEG. *Front Psychol* **2**, 51 (2011).
8. Dinstein I, Heeger DJ, Behrmann M. Neural variability: friend or foe? *Trends Cogn Sci* **19**, 322-328 (2015).
9. Haigh SM, Minshew N, Heeger DJ, Dinstein I, Behrmann M. Over-Responsiveness and Greater Variability in Roughness Perception in Autism. *Autism Res* **9**, 393-402 (2016).
10. Kovarski K, Malvy J, Khanna RK, Arsene S, Batty M, Latinus M. Reduced visual evoked potential amplitude in autism spectrum disorder, a variability effect? *Transl Psychiatry* **9**, 341 (2019).
11. Latinus M, Mofid Y, Kovarski K, Charpentier J, Batty M, Bonnet-Brilhault F. Atypical Sound Perception in ASD Explained by Inter-Trial (In)consistency in EEG. *Front Psychol* **10**, 1177 (2019).
12. Haigh SM. Variable sensory perception in autism. *Eur J Neurosci* **47**, 602-609 (2018).
13. Rubenstein JL, Merzenich MM. Model of autism: increased ratio of excitation/inhibition in key neural systems. *Genes Brain Behav* **2**, 255-267 (2003).
14. Baron-Cohen S*, et al.* Is synaesthesia more common in autism? *Mol Autism* **4**, 40 (2013).
15. Ward J. Individual differences in sensory sensitivity: A synthesizing framework and evidence from normal variation and developmental conditions. *Cogn Neurosci* **10**, 139-157 (2019).
16. Simmons DR, Robertson AE, McKay LS, Toal E, McAleer P, Pollick FE. Vision in autism spectrum disorders. *Vision Res* **49**, 2705-2739 (2009).
17. Uljarevic M, Baranek G, Vivanti G, Hedley D, Hudry K, Lane A. Heterogeneity of sensory features in autism spectrum disorder: Challenges and perspectives for future research. *Autism Res* **10**, 703-710 (2017).
18. Robertson CE, Baron-Cohen S. Sensory perception in autism. *Nat Rev Neurosci* **18**, 671-684 (2017).
19. Wallace MT, Woynaroski TG, Stevenson RA. Multisensory Integration as a Window into Orderly and Disrupted Cognition and Communication. *Annu Rev Psychol* **71**, 193-219 (2020).
20. O'Hare L, Hibbard PB. Visual processing in migraine. *Cephalalgia* **36**, 1057-1076 (2016).
21. Faisal AA, Selen LP, Wolpert DM. Noise in the nervous system. *Nat Rev Neurosci* **9**, 292-303 (2008).
22. Faisal AA. Noise in Neurons and Other Constraints. In: *Computational Systems Neurobiology* (ed Le Novère N). Springer Netherlands (2012).

23. Simmons D, Milne E. Response to Davis and Plaisted-Grant: low or high endogenous neural noise in autism spectrum disorder? *Autism* **19**, 363-364 (2015).
24. Davis G, Plaisted-Grant K. Low endogenous neural noise in autism. *Autism* **19**, 351-362 (2015).
25. Sinclair D, Oranje B, Razak KA, Siegel SJ, Schmid S. Sensory processing in autism spectrum disorders and Fragile X syndrome-From the clinic to animal models. *Neurosci Biobehav Rev* **76**, 235-253 (2017).
26. Abraira VE, Ginty DD. The sensory neurons of touch. *Neuron* **79**, 618-639 (2013).
27. Bryant LK, Woynaroski TG, Wallace MT, Cascio CJ. Self-reported Sensory Hypersensitivity Moderates Association Between Tactile Psychophysical Performance and Autism-Related Traits in Neurotypical Adults. *J Autism Dev Disord* **49**, 3159-3172 (2019).
28. Morrison I, Loken LS, Olausson H. The skin as a social organ. *Exp Brain Res* **204**, 305-314 (2010).
29. Quiquempoix M, Fayad SL, Boutourlinsky K, Leresche N, Lambert RC, Bessaih T. Layer 2/3 Pyramidal Neurons Control the Gain of Cortical Output. *Cell Rep* **24**, 2799-2807 e2794 (2018).
30. Velmeshev D*, et al.* Single-cell genomics identifies cell type-specific molecular changes in autism. *Science* **364**, 685-689 (2019).
31. Shadlen MN, Newsome WT. The variable discharge of cortical neurons: implications for connectivity, computation, and information coding. *J Neurosci* **18**, 3870-3896 (1998).
32. Azouz R, Gray CM. Cellular mechanisms contributing to response variability of cortical neurons in vivo. *J Neurosci* **19**, 2209-2223 (1999).
33. Lin IC, Okun M, Carandini M, Harris KD. The Nature of Shared Cortical Variability. *Neuron* **87**, 644-656 (2015).
34. Magee JC. Dendritic integration of excitatory synaptic input. *Nat Rev Neurosci* **1**, 181-190 (2000).
35. White JA, Rubinstein JT, Kay AR. Channel noise in neurons. *Trends Neurosci* **23**, 131-137 (2000).
36. Engel AK, Fries P, Singer W. Dynamic predictions: oscillations and synchrony in top-down processing. *Nat Rev Neurosci* **2**, 704-716 (2001).
37. Buzsaki G, Draguhn A. Neuronal oscillations in cortical networks. *Science* **304**, 1926-1929 (2004).
38. Jonak CR, Lovelace JW, Ethell IM, Razak KA, Binder DK. Multielectrode array analysis of EEG biomarkers in a mouse model of Fragile X Syndrome. *Neurobiol Dis* **138**, 104794 (2020).
39. Petersen CC, Hahn TT, Mehta M, Grinvald A, Sakmann B. Interaction of sensory responses with spontaneous depolarization in layer 2/3 barrel cortex. *Proc Natl Acad Sci U S A* **100**, 13638-13643 (2003).
40. Sachdev RN, Ebner FF, Wilson CJ. Effect of subthreshold up and down states on the whisker-evoked response in somatosensory cortex. *J Neurophysiol* **92**, 3511-3521 (2004).
41. Ringach DL. Spontaneous and driven cortical activity: implications for computation. *Curr Opin Neurobiol* **19**, 439-444 (2009).
42. Chacron MJ, Longtin A, Maler L. The effects of spontaneous activity, background noise, and the stimulus ensemble on information transfer in neurons. *Network* **14**, 803-824 (2003).

43. Barth AL, Poulet JF. Experimental evidence for sparse firing in the neocortex. *Trends Neurosci* **35**, 345-355 (2012).
44. Bhaskaran AA, Bony G, Le Corf K, Frick A. Sensory stimulus evoked responses in layer 2/3 pyramidal neurons of the hind paw-related mouse primary somatosensory cortex. *bioRxiv*, (2020).
45. Deng PY*, et al.* FMRP regulates neurotransmitter release and synaptic information transmission by modulating action potential duration via BK channels. *Neuron* **77**, 696-711 (2013).
46. Zhang Y*, et al.* Dendritic channelopathies contribute to neocortical and sensory hyperexcitability in Fmr1(-/y) mice. *Nat Neurosci* **17**, 1701-1709 (2014).
47. Larkum ME. A new cellular mechanism for coupling inputs arriving at different cortical layers. *Nature* **398**, (1999).
48. Hahamy A, Behrmann M, Malach R. The idiosyncratic brain: distortion of spontaneous connectivity patterns in autism spectrum disorder. *Nat Neurosci* **18**, 302-309 (2015).
49. Haberl MG, Zerbi V, Veltien A, Ginger M, Heerschap A, Frick A. Structural-functional connectivity deficits of neocortical circuits in the Fmr1 (-/y) mouse model of autism. *Sci Adv* **1**, e1500775 (2015).
50. Keown CL, Shih P, Nair A, Peterson N, Mulvey ME, Muller RA. Local functional overconnectivity in posterior brain regions is associated with symptom severity in autism spectrum disorders. *Cell Rep* **5**, 567-572 (2013).
51. Zerbi V*, et al.* Brain mapping across 16 autism mouse models reveals a spectrum of functional connectivity subtypes. *Mol Psychiatry*, (2021).
52. Laumonnier F*, et al.* Association of a functional deficit of the BKCa channel, a synaptic regulator of neuronal excitability, with autism and mental retardation. *Am J Psychiatry* **163**, 1622-1629 (2006).
53. Zaman T, De Oliveira C, Smoka M, Narla C, Poulter MO, Schmid S. BK Channels Mediate Synaptic Plasticity Underlying Habituation in Rats. *J Neurosci* **37**, 4540-4551 (2017).
54. Mori A, Suzuki S, Sakamoto K, Nakahara T, Ishii K. BMS-191011, an opener of large-conductance Ca2+-activated potassium channels, dilates rat retinal arterioles in vivo. *Biol Pharm Bull* **34**, 150-152 (2011).
55. Waschke L, Kloosterman NA, Obleser J, Garrett DD. Behavior needs neural variability. *Neuron* **109**, 751-766 (2021).
56. Goncalves JT, Anstey JE, Golshani P, Portera-Cailliau C. Circuit level defects in the developing neocortex of Fragile X mice. *Nat Neurosci* **16**, 903-909 (2013).
57. Kwon SE. The Interplay Between Cortical State and Perceptual Learning: A Focused Review. *Front Syst Neurosci* **12**, 47 (2018).
58. Compte A, Reig R, Descalzo VF, Harvey MA, Puccini GD, Sanchez-Vives MV. Spontaneous high-frequency (10-80 Hz) oscillations during up states in the cerebral cortex in vitro. *J Neurosci* **28**, 13828-13844 (2008).
59. Buzsaki G, Wang XJ. Mechanisms of gamma oscillations. *Annu Rev Neurosci* **35**, 203-225 (2012).

60. Donoghue T*, et al.* Parameterizing neural power spectra into periodic and aperiodic components. *Nat Neurosci* **23**, 1655-1665 (2020).
61. Simon DM, Wallace MT. Dysfunction of sensory oscillations in Autism Spectrum Disorder. *Neurosci Biobehav Rev* **68**, 848-861 (2016).
62. Ethridge LE*, et al.* Auditory EEG Biomarkers in Fragile X Syndrome: Clinical Relevance. *Front Integr Neurosci* **13**, 60 (2019).
63. Pedapati EV*, et al.* Neocortical localization and thalamocortical modulation of neuronal hyperexcitability contribute to Fragile X Syndrome. *Commun Biol* **5**, 442 (2022).
64. Goswami S, Cavalier S, Sridhar V, Huber KM, Gibson JR. Local cortical circuit correlates of altered EEG in the mouse model of Fragile X syndrome. *Neurobiol Dis* **124**, 563-572 (2019).
65. McDonnell MD, Abbott D. What is stochastic resonance? Definitions, misconceptions, debates, and its relevance to biology. *PLoS Comput Biol* **5**, e1000348 (2009).
66. Destexhe A. Noise Enhancement of Neural Information Processing. *Entropy (Basel)* **24**, (2022).
67. Ward LM, Neiman A, Moss F. Stochastic resonance in psychophysics and in animal behavior. *Biol Cybern* **87**, 91-101 (2002).
68. D R Simmons LM, P McAleer, E Toal, A Robertson, F E Pollick. Neural noise and autism spectrum disorders. (2007).
69. Simmons DR. Some clarifications on neural noise and sensory sensitivities in Autism. *Cogn Neurosci* **10**, 169-171 (2019).
70. Rosenberg A, Patterson JS, Angelaki DE. A computational perspective on autism. *Proc Natl Acad Sci U S A* **112**, 9158-9165 (2015).
71. Carandini M, Heeger DJ. Normalization as a canonical neural computation. *Nat Rev Neurosci* **13**, 51-62 (2011).
72. Juczewski K, von Richthofen H, Bagni C, Celikel T, Fisone G, Krieger P. Somatosensory map expansion and altered processing of tactile inputs in a mouse model of fragile X syndrome. *Neurobiol Dis* **96**, 201-215 (2016).
73. Rotschafer S, Razak K. Altered auditory processing in a mouse model of fragile X syndrome. *Brain Res* **1506**, 12-24 (2013).
74. Cascio CJ, Gu C, Schauder KB, Key AP, Yoder P. Somatosensory Event-Related Potentials and Association with Tactile Behavioral Responsiveness Patterns in Children with ASD. *Brain Topogr* **28**, 895-903 (2015).
75. Ward J*, et al.* Atypical sensory sensitivity as a shared feature between synaesthesia and autism. *Sci Rep* **7**, 41155 (2017).
76. Rojas DC, Wilson LB. gamma-band abnormalities as markers of autism spectrum disorders. *Biomark Med* **8**, 353-368 (2014).
77. Kaiser MD*, et al.* Brain Mechanisms for Processing Affective (and Nonaffective) Touch Are Atypical in Autism. *Cereb Cortex* **26**, 2705-2714 (2016).

78. Khan S*, et al.* Altered Onset Response Dynamics in Somatosensory Processing in Autism Spectrum Disorder. *Front Neurosci* **10**, 255 (2016).
79. Green SA, Hernandez L, Tottenham N, Krasileva K, Bookheimer SY, Dapretto M. Neurobiology of Sensory Overresponsivity in Youth With Autism Spectrum Disorders. *JAMA Psychiatry* **72**, 778-786 (2015).
80. Espenhahn S*, et al.* Tactile cortical responses and association with tactile reactivity in young children on the autism spectrum. *Mol Autism* **12**, 26 (2021).
81. Carreno-Munoz MI*, et al.* Potential Involvement of Impaired BKCa Channel Function in Sensory Defensiveness and Some Behavioral Disturbances Induced by Unfamiliar Environment in a Mouse Model of Fragile X Syndrome. *Neuropsychopharmacology* **43**, 492-502 (2018).
82. Hebert B*, et al.* Rescue of fragile X syndrome phenotypes in Fmr1 KO mice by a BKCa channel opener molecule. *Orphanet J Rare Dis* **9**, 124 (2014).
83. Zhaoping L. Theoretical understanding of the early visual processes by data compression and data selection. *Network* **17**, 301-334 (2006).
84. Antoine MW, Langberg T, Schnepel P, Feldman DE. Increased Excitation-Inhibition Ratio Stabilizes Synapse and Circuit Excitability in Four Autism Mouse Models. *Neuron* **101**, 648-661 e644 (2019).
85. Markram K, Markram H. The intense world theory - a unifying theory of the neurobiology of autism. *Front Hum Neurosci* **4**, 224 (2010).
86. Nelson SB, Valakh V. Excitatory/Inhibitory Balance and Circuit Homeostasis in Autism Spectrum Disorders. *Neuron* **87**, 684-698 (2015).
87. Kristen Bottema-Beutel SKK, Jessica Nina Lester, Noah J. Sasson, and Brittany N. Hand. Avoiding Ableist Language: Suggestions for Autism Researchers. *Autism in Adulthood* **3**, 18-29 (2021).

Figures

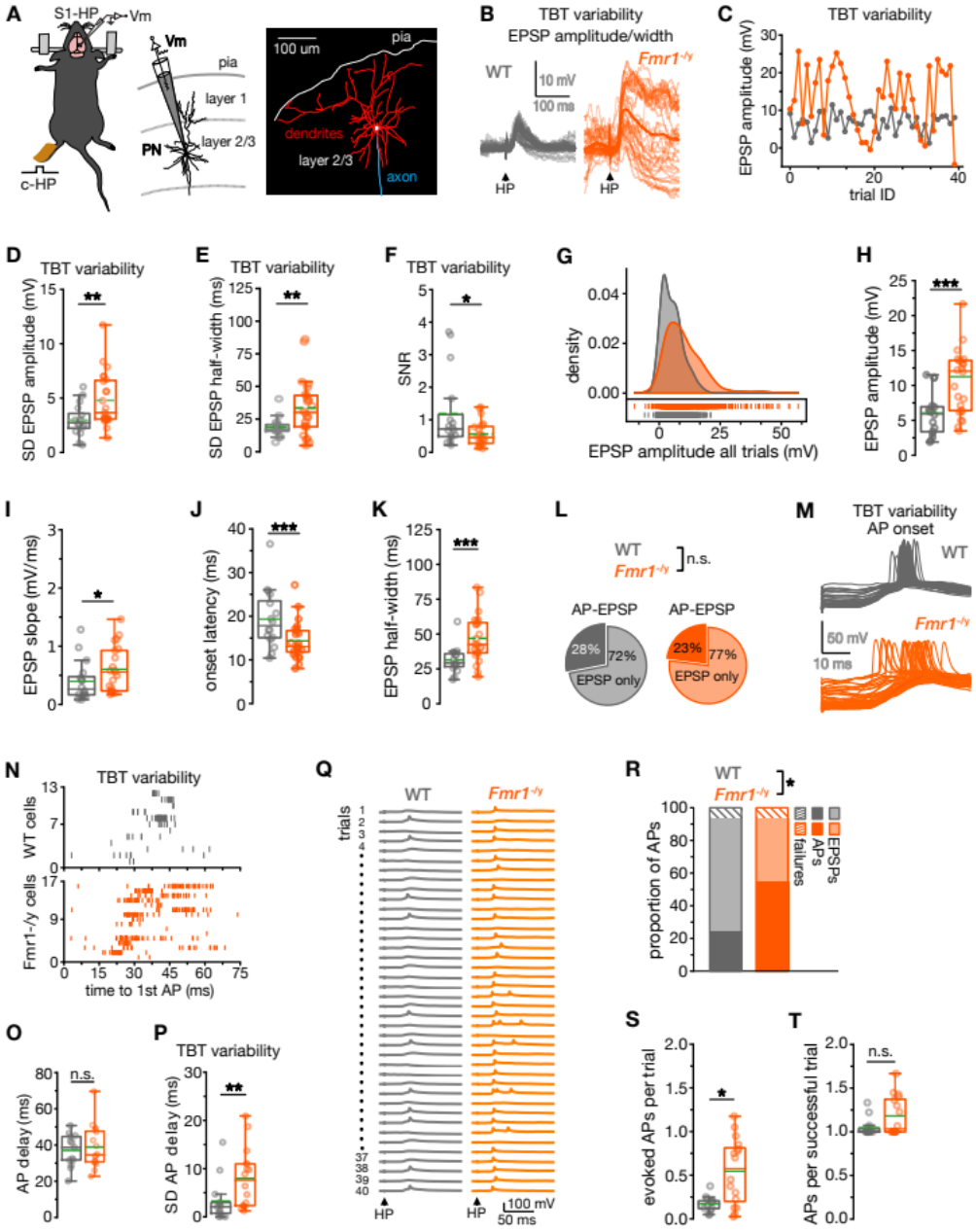

Figure 1

Trial-by-trial variability of sensory responses is markedly increased in S1–L2/3 pyramidal neurons of Fmr1$^{-/y}$ mice.

(A) *Experimental setup. Sensory stimulus evoked activity was recorded in L2/3 pyramidal neurons of the hindpaw related S1 (S1–HP) region during contralateral HP stimulation (left). Morphological*

reconstruction (right) of a recorded neuron. ***(B-K)*** *Analysis for n = 24 cells from 14 mice for Fmr1$^{-/y}$ neurons and n = 16 cells from 7 mice for WT mice.* ***(B–F)*** *Trial–by–trial (TBT) variability of EPSPs.* ***(B)*** *Example of trial-by-trial variability of EPSP amplitudes across 40 trials for one WT and one Fmr1$^{-/y}$ cell. Average responses are shown in darker colour.* ***(C)*** *Same traces from panel B, plotted versus number of trials. Standard deviation (SD) of* ***(D)*** *EPSP amplitudes and* ***(E)*** *EPSP half-width across trials were larger for Fmr1$^{-/y}$ neurons.* ***(F)*** *Signal–to–noise ratio (SNR) of EPSP responses (EPSP amplitude divided by response variance across trials).* ***(G)*** *Density plot showing the different distribution of EPSP amplitude values for both genotypes. Box plots demonstrating larger EPSP amplitudes* ***(H)****, enhanced EPSP rise slope* ***(I)****, shorter onset latency of EPSPs (following stimulus)* ***(J)****, and a greater EPSP half–width* ***(K)*** *for Fmr1$^{-/y}$ neuron population.* ***(L)*** *Pie charts showing proportion of neurons responding with APs in some of the trials (AP–EPSP neurons), and of those responding with EPSPs only (EPSP only neurons).* ***(M–P)*** *Trial-by-trial onset variability of AP onset following HP stimulation. (AP–EPSP neurons; Fmr1$^{-/y}$, n = 16 cells from 15 mice; WT, n = 14 cells from 12 mice).* ***(M)*** *Example traces of HP stimulus evoked AP responses in an individual WT and Fmr1$^{-/y}$ neuron showing different temporal dispersion of first evoked AP.* ***(N)*** *Onset of each first AP across 40 HP-stimulation trials indicated for all AP-EPSP neurons.* ***(O)*** *No genotype difference of trial-wise average of AP delay.* ***(P)*** *Greater trial–by–trial AP jitter for Fmr1$^{-/y}$ neurons.* ***(Q–T)*** *Properties of HP stimulus evoked APs.* ***(Q)*** *Example of responses to 40 successive HP stimuli in a WT and a Fmr1$^{-/y}$ AP–EPSP neuron.* ***(R)*** *Stacked bar graph showing percentage for each response outcome (APs, EPSPs, failures) to HP stimuli for the AP-EPSP responding neurons.* ***(S)*** *Box plots showing increased number of evoked APs averaged across all 40 trials in Fmr1$^{-/y}$ neurons.* ***(T)*** *Number of APs per successful trial (i.e., AP evoking trial) were not different between genotypes. Box-and-whisker plots show the median, interquartile range, range, mean (green line) and individual values. Statistical significance was calculated using unpaired t-test (J, O), Fisher's exact test (L),Chi-square 3x3 test (R) or Mann-Whitney U-test (D, E, F, H, I, J, K, P, S, T). n.s., not significant, *P < 0.05, **P < 0.01, ***P < 0.001.*

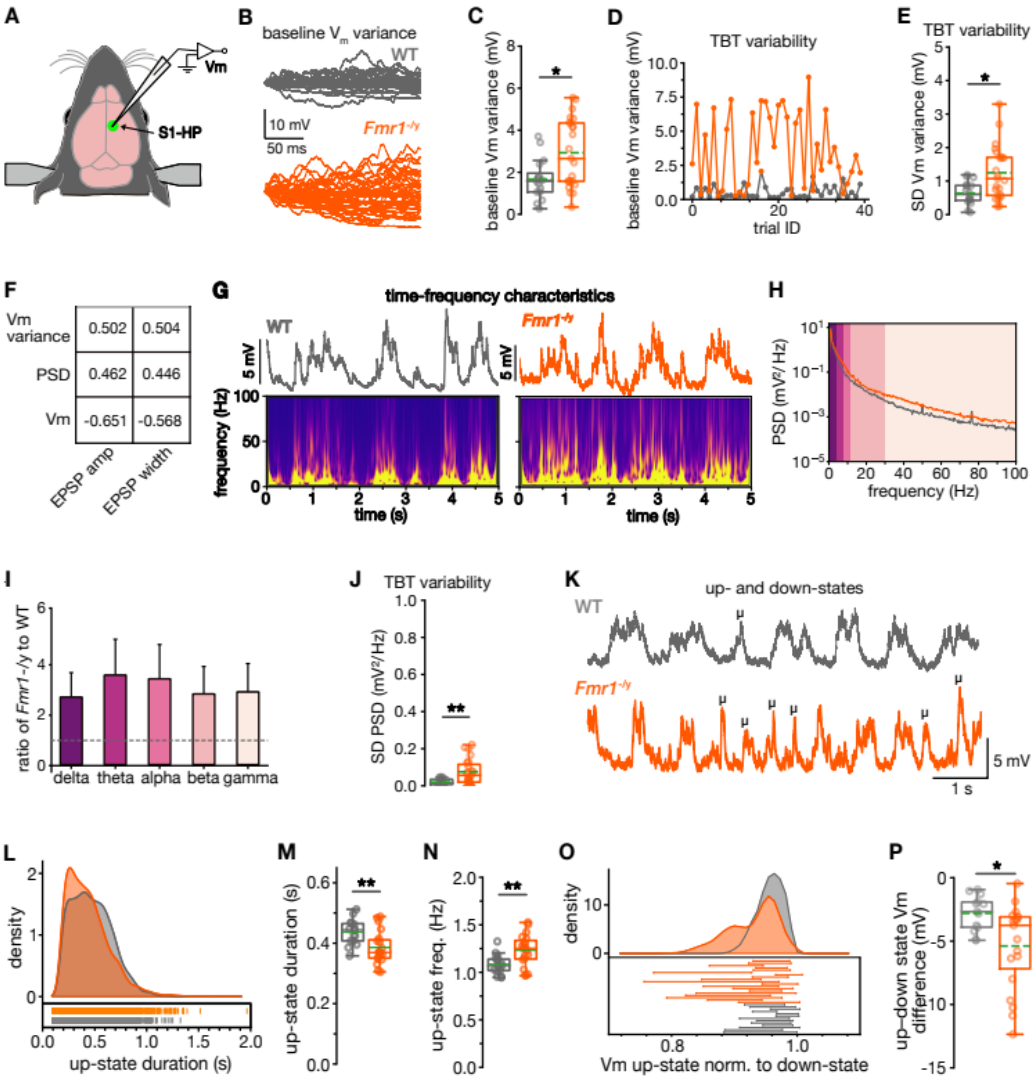

Figure 2

Endogenous neural noise drives trial-by-trial variability of sensory responses.

(A) *Experimental setup. Whole-cell recordings of L2/3 pyramidal neurons of the S1–HP region* ***(B–J)*** *Fluctuation of the membrane potential (V_m variance). ($Fmr1^{-/y}$, n = 23 cells from 14 mice; WT, n = 16 cells from 7 mice)* ***(B)*** *Example for baseline (200-ms time window just before the onset of the HP stimulus) V_m*

variance for a WT and a Fmr1$^{-/y}$ neuron. ***(C)*** *Baseline V_m variance was exaggerated for Fmr1$^{-/y}$ neurons.* ***(D)*** *Baseline V_m variance for same trials as shown in B and Fig. 1C, showing enhanced intra–cell variability in Fmr1$^{-/y}$ neurons and correlation with EPSP amplitude.* ***(E)*** *Exaggerated trial–by–trial variability in baseline V_m variance (SD of baseline V_m variance) for Fmr1$^{-/y}$ neurons.* ***(F)*** *Correlation of baseline V_m variance, power spectral density (PSD) and V_m (all calculated during 200-ms time window before HP stimulus onset) with EPSP amplitude and EPSP half–width on a trial–by–trial basis. Baseline V_m variance and PSD were normalized by V_m.* ***(G–J)*** *PSD. (Fmr1$^{-/y}$, n = 23 cells from 14 mice; WT, n = 16 cells from 7 mice)* ***(G)*** *Example of power–time–frequency characteristics of V_m calculated using wavelet transformation illustrating higher frequency components during up–states.* ***(H)*** *Power spectral density (PSD) across a frequency spectrum of 0–100 Hz.* ***(I)*** *Fmr1$^{-/y}$-to-WT PSD ratio for different frequency bands: delta (1–4 Hz), theta (4–8 Hz), alpha (8–12 Hz), beta (12–30 Hz), gamma (30–100 Hz).* ***(J)*** *Increased trial-by-trial variability of baseline PSD for the Fmr1$^{-/y}$ neuron population.* ***(K–P)*** *Up– and down–states (Fmr1$^{-/y}$, n = 19 cells from 16 mice; WT, n = 13 cells from 8 mice).* ***(K)*** *Example traces from a WT and a Fmr1$^{-/y}$ L2/3 pyramidal neuron. Note predominant occurrence of short-duration (100–150ms) up–states in the Fmr1$^{-/y}$ but not WT neuron (marked with* ***μ****).* ***(L)*** *Density distribution histogram of up–state duration for the Fmr1$^{-/y}$ and WT neuron population. Box plots of up–state duration* ***(M)*** *and up–state frequency* ***(N). (O)*** *Density distribution histogram of up-state (V_m) normalized to mean downstate (Vm).* ***(P)*** *Box plot of up–down state membrane potential (V_m) difference. Box-and-whisker plots show the median, interquartile range, range, mean (green line) and individual values. Statistical significance was calculated using unpaired t–test (M, N and P), Mann-Whitney U test (C, E), Pearson R test(F). n.s., not significant, *P < 0.05, **P<0.01.*

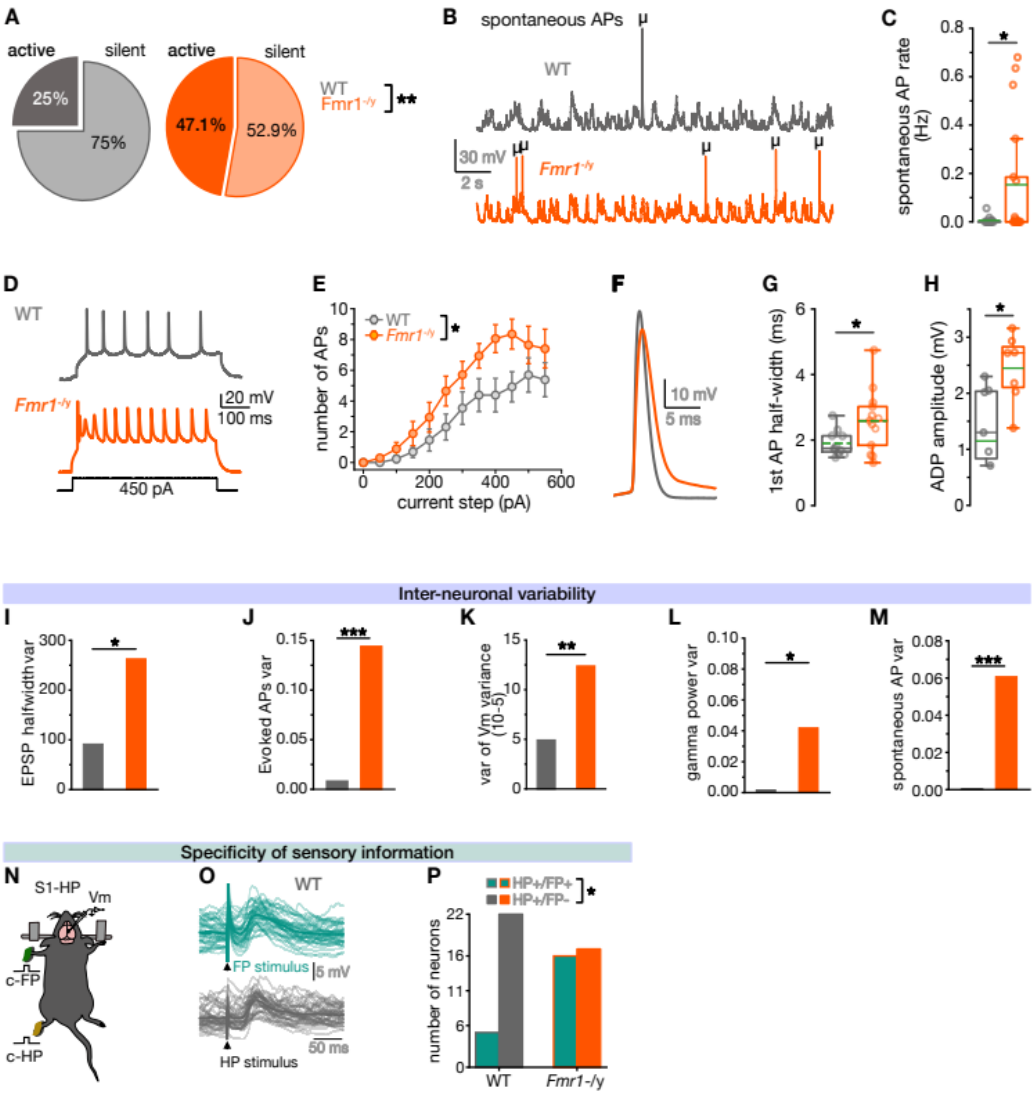

Figure 3

Changes in action potential properties, inter-neuronal variability, and receptive field specificity in Fmr1$^{-/y}$ mice.

(A–C) *Spontaneous AP activity (Fmr1$^{-/y}$, n = 17 cells from 15 mice; WT, n = 16 cells from 10 mice).* ***(A)*** *Pie charts showing percentage of neurons that were spontaneously active (dark color) or silent (light color)*

during a time window of 120 s. ***(B)*** *Representative example traces from a WT (grey) and a Fmr1$^{-/y}$ L2/3 pyramidal neuron (orange); µ-symbols indicate spontaneous action potentials (AP).* ***(C)*** *Box plot showing increased AP frequency in Fmr1$^{-/y}$ neurons.* ***(D–H)*** *Intrinsic properties.* ***(D)*** *Example voltage traces in response to a depolarizing current step for a WT and a Fmr1$^{-/y}$ neuron.* ***(E)*** *Mean number of APs plotted as function of the injected current (Fmr1$^{-/y}$, n = 17 cells from 16 mice; WT, n = 13 cells from 8 mice).* ***(F)*** *Example traces showing the increased broadening of APs for a Fmr1$^{-/y}$ compared to WT neuron.* ***(G)*** *Box plot showing the first AP half–width (Fmr1$^{-/y}$, n = 15 cells from 11 mice; WT, n = 11 cells from 7 mice).* ***(H)*** *Average amplitude of after-depolarization (ADP) (Fmr1$^{-/y}$, n = 7 cells from 3 mice; WT, n = 7 cells from 2 mice).* ***(I-M)*** *Inter-neuronal variability across cell population. Bar graphs illustrating increased variance of EPSP half-width (analysis for n = 24 cells from 14 mice for Fmr1$^{-/y}$ neurons and n = 16 cells from 7 mice for WT mice)* ***(I)****, HP stimulus evoked APs (Fmr1$^{-/y}$, n = 16 cells from 14 mice; WT, n = 14 cells from 12 mice)* ***(J),*** *V_m variance (Fmr1$^{-/y}$, n = 23 cells from 14 mice; WT, n = 16 cells from 7 mice)* ***(K)****, gamma power (n = 24 cells from 14 mice for Fmr1$^{-/y}$ neurons and n = 16 cells from 7 mice for WT mice)* ***(L)****, and of spontaneous APs (Fmr1$^{-/y}$, n = 17 cells from 15 mice; WT, n = 16 cells from 10 mice)* ***(M)*** *for the Fmr1$^{-/y}$ neuron population.* ***(N–P)*** *Receptive field changes of S1–HP L2/3 pyramidal neurons (Fmr1$^{-/y}$, n = 33 cells from 28 mice; WT, n = 27 cells from 23 mice).* ***(N)*** *Schematic of experimental condition illustrating stimulation of both HP and forepaw (FP) while recording from S1-HP neurons.* ***(O)*** *Example for HP and FP stimulus evoked responses in the same WT neuron.* ***(P)*** *Number of neurons responding to HP–only stimulus and to HP/FP stimuli in WT and Fmr1$^{-/y}$ mice. Box-and-whisker plots show the median, interquartile range, range, mean (green line) and individual values. Statistical significance was calculated using unpaired t–test (G and H), or mixed ANOVA (E), Bartlett variance test (I), Levene variance test (K and M), F test (J), Two–sided permutation test (C), Fisher's exact test (P). n.s., not significant, *P < 0.05, **P<0.01.*

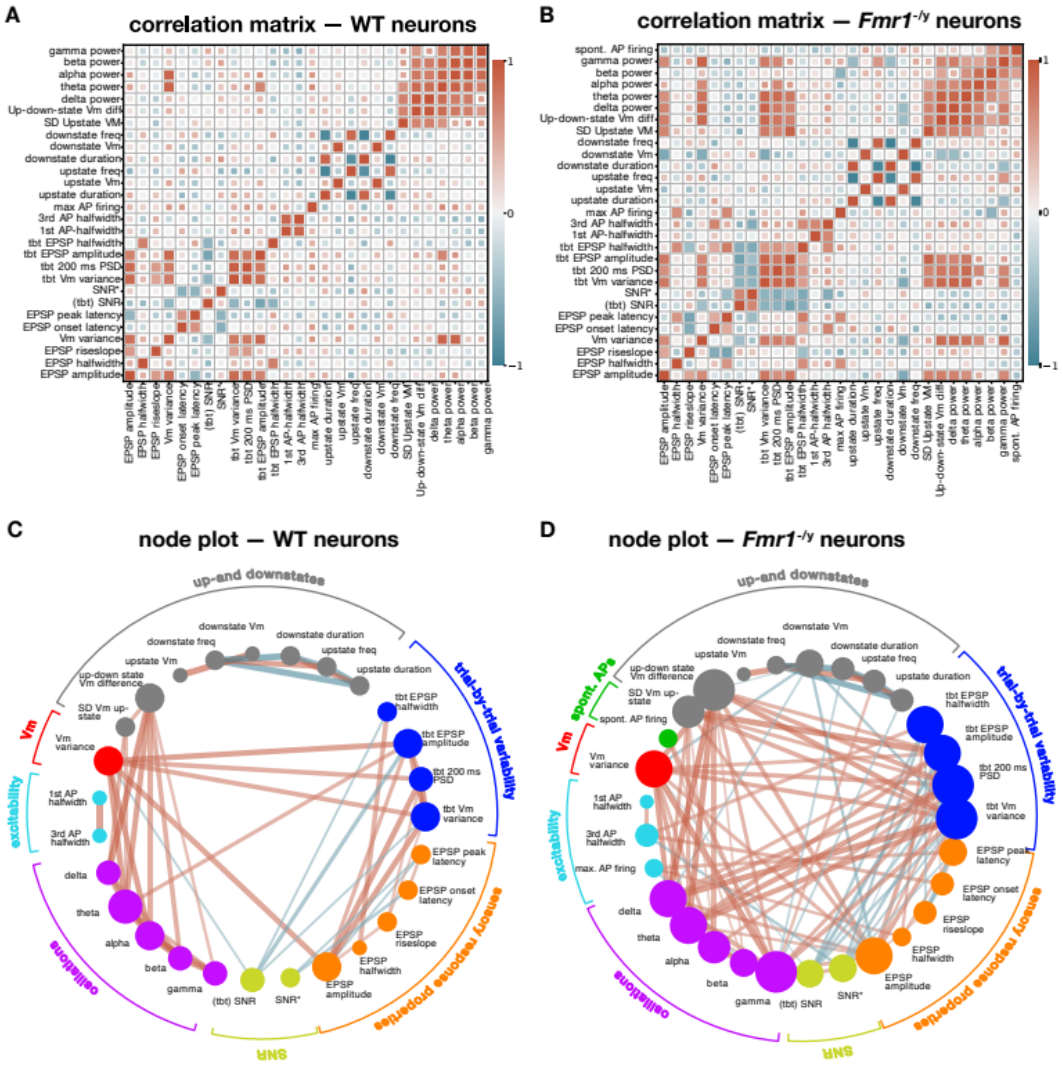

Figure 4

Stronger correlation of endogenous noise with sensory response variability in Fmr1$^{-/y}$ neurons. (A, B) *Correlation of main parameters describing spontaneous AP firing, up-/down−state pattern, intrinsic excitability, power−spectral−density, HP stimulus evoked responses and trial−by−trial (tbt) variability. Positive correlations are indicated in red and negative correlations in blue. The correlation strength is color-coded, and statistically significant correlations are indicated by large squares. Correlation matrix of*

*WT neurons **(A)**, and Fmr1$^{-/y}$ neurons **(B)**. **(C, D)** Node graphs displaying only the statistically significant correlations of the main parameters. The size of the node is proportional to the number of significant correlations with other parameters. The thickness of the edges is proportional to the coefficient (strength) of the correlation. The parameters have been grouped under the same color according to their biological similarities. Node graph of WT **(C)**, and Fmr1$^{-/y}$ **(D)** neurons.*

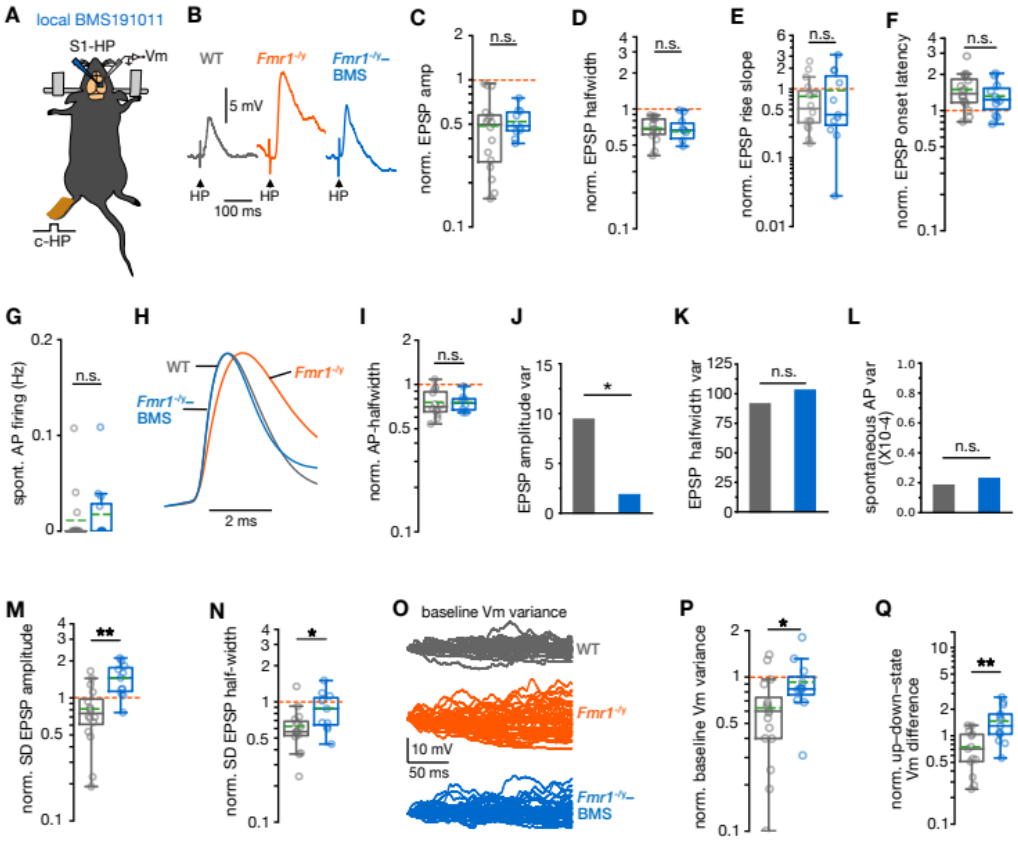

Figure 5

Dissecting the origin of noise sources by targeting local neocortical ion channel dysfunction. (A) *Schematic of local BMS191011 (abbreviated BMS) application onto S1, combined with whole-cell recordings from HP stimulus evoked responses.* ***(B)*** *Example traces of HP stimulus evoked EPSPs from a WT–, Fmr1$^{-/y}$– and a Fmr1$^{-/y}$ neuron in the presence of BMS (Fmr1-/y–BMS neuron) revealing correction of EPSP amplitude and half-width by BMS191011.* ***(C-F, I, M, N, P, Q)*** *Fmr1$^{-/y}$–BMS and WT values were normalized to those of Fmr1$^{-/y}$ neurons and statistically compared to test for correction.* ***(C–F)*** *EPSP features (Fmr1$^{-/y}$–BMS, n = 10 cells from 10 mice). Box plots showing correction of EPSP amplitude* ***(C)****, EPSP half-width* ***(D)****, EPSP rise slope* ***(E)****, and EPSP onset latency* ***(F)*** *in the Fmr1$^{-/y}$ neuron population.* ***(G)*** *Correction of spontaneous AP firing (Fmr1$^{-/y}$–BMS, n = 12 cells from 12 mice).* ***(H)*** *Example traces of APs from a WT–, Fmr1$^{-/y}$– and a Fmr1$^{-/y}$–BMS neuron demonstrating correction of 1st AP halfwidth by BMS191011. APs were scaled to the peak to visualize differences in halfwidth.* ***(I)*** *Box plot showing correction of AP half–width of Fmr1$^{-/y}$ neurons (Fmr1$^{-/y}$–BMS, n = 8 cells from 8 mice).* ***(J-L)*** *Inter-neuronal variability.* ***(J)*** *Bar graph demonstrating reduction in inter-neuronal variability of EPSP amplitude below that of WT neurons. Correction of inter-neuronal variability of EPSP half-width* ***(K)*** *and of spontaneous AP firing* ***(L)****.* ***(M)*** *Increase in trial-by-trial variability of EPSP amplitude.* ***(N)*** *Lack of correction of trial–by–trial variability in EPSP half-width.* ***(O)*** *Example traces of baseline V_m variance from a WT–, Fmr1$^{-/y}$– and a Fmr1$^{-/y}$–BMS neuron under the three different conditions.* ***(P)*** *Lack of correction of atypical baseline V_m variance by BMS191011. (****Q****) Lack of correction of Upstate-Downstate Vm difference by BMS191011. (Box-and-whisker plots show the median, interquartile range, range, mean (green line) and individual values. Data was normalized to mean (C, D, I, F, Q) or median (E, G, M, N, P), Statistical significance was calculated using unpaired t-test (C, D, I, F, Q), Mann-Whitney U test (E, M, N, P) or Two sided permutation test (G), Bartlett test (J), Levene test (K, L). n.s., not significant, *P < 0.05, **P < 0.01, ***P < 0.001.*

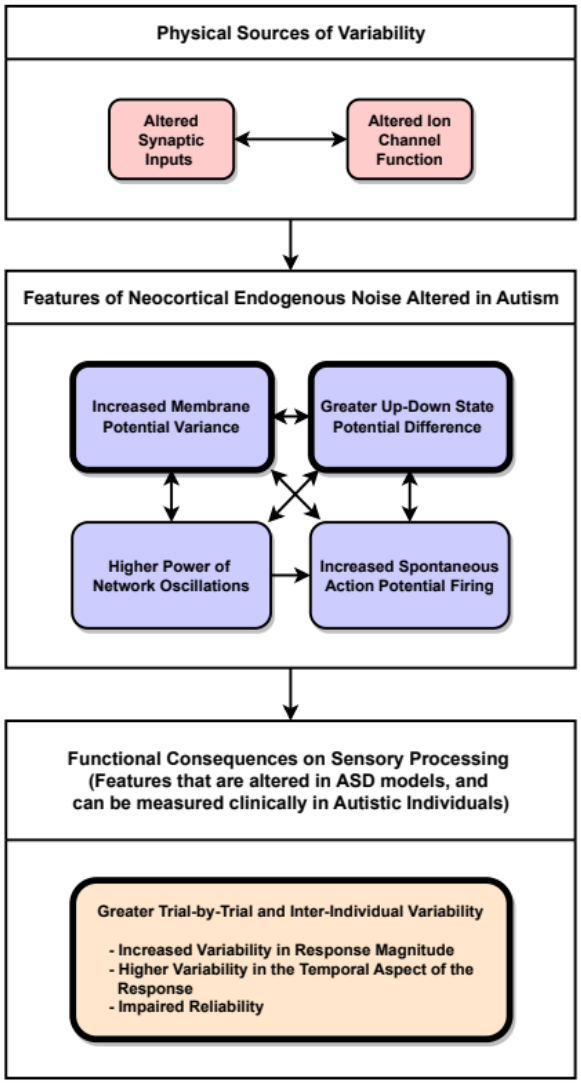

Figure 6

Model of the relationship between endogenous noise features and atypical sensory processing. *The schematic highlights the physical sources and main features of endogenous neural noise in Fmr1$^{-/y}$ neurons of the S1-HP cortex, their inter-relationships, as well as their impact on atypical sensory processing. These alterations provide an explanation for the nuanced and complex sensory symptomatology in autistic individuals. This demonstrates not only features that are altered in our*

autism model but also potential translational biomarkers that can be measured both in clinical and preclinical settings. These measures include the strength, onset, duration and variability of sensory responses. The oscillation power could also be measured clinically under basal conditions and during sensory processing. In addition, endogenous noise could also partly be measured in humans, e.g. by measuring the background activity before the onset of sensory responses. Our schematic also provides a framework for the evaluation of drug application for noise and ensuing atypical sensory information processing in autism.

Supplementary Files

This is a list of supplementary files associated with this preprint. Click to download.

- SupplementaryTableS1.Dataorganized.xlsx
- reportingsummarynew.pdf